Molecular Therapy
Original Article

AAV-delivered PPT1 provides long-term neurological benefits in CLN1 mice and achieves therapeutic levels in sheep brain

Md Suhail Alam,[1] Apeksha Khatiwada,[1] Samantha L. Eaton,[2] Daniel M. Cohen,[1] John White,[1] Melissa Derby,[1] Drew Peterson,[1] Graciela Rivera-Pena,[1] Mohamad Nayal,[1] Mallory Becker,[1] Heena Beck,[1] Charlie Li,[1] Renee Gentzel,[1] George Atkins,[1] Stephen N. Greenhalgh,[2,3] Simon G. Lillico,[2] Rachael Gregson,[2,3] Eddie Clutton,[2,3] Fraser Murdoch,[2] James Nixon,[3] Mark Gray,[2,3] Gerard Thompson,[4] Jodi McBride,[1] Thomas M. Wishart,[2,5] Maria Grazia Biferi,[1] and Elizabeth Ramsburg[1]

[1]Spark Therapeutics Inc., Philadelphia, PA 19104, USA; [2]The Roslin Institute and Royal (Dick) School of Veterinary Studies, University of Edinburgh, Edinburgh EH25 9RG, UK; [3]Large Animal Research and Imaging Facility, University of Edinburgh, Edinburgh EH25 9RG, UK; [4]Centre for Clinical Brain Sciences, University of Edinburgh, Edinburgh EH16 4SB, UK; [5]Centre for Systems Health and Integrated Metabolic Research, Department of Biosciences, School of Science and Technology Nottingham Trent University, Nottingham NG1 4GG, UK

CLN1 disease is a fatal neurodegenerative condition caused by deficiency in palmitoyl-protein thioesterase 1 (PPT1), for which no disease-modifying therapy exists. The disease affects the entire central nervous system (CNS), necessitating widespread delivery of therapeutics to the brain and spinal cord. Adeno-associated virus (AAV)-based PPT1 gene therapy delivered intrathecally has been tested in mouse models but has shown limited efficacy due to inadequate brain bioavailability. Here, to maximize therapeutic benefit, PPT1 was engineered for improved cross-correction capabilities, packaged in Spark100, a neurotropic AAV capsid, and administered through intracerebroventricular route in neonatal *Ppt1*$^{-/-}$ mice. This achieved sustained expression of PPT1 protein across the CNS, including key disease-relevant structures, for up to 15 months. It resulted in long-term therapeutic benefits, such as extended lifespan, preserved neurobehavioral function, and prevention of neuropathology, making treated *Ppt1*$^{-/-}$ mice nearly indistinguishable from wild type. A translatability study in healthy adult sheep, assessing biodistribution of therapeutic in a large and fully developed brain, showed widespread CNS transduction and PPT1 expression with no adverse effects. These studies demonstrate the potential of this approach for treating CLN1 disease and suggest that a similar platform, using a secreted therapeutic protein, might apply to other neurological disorders with broad CNS deficits.

INTRODUCTION

Neuronal ceroid lipofuscinoses (NCLs), commonly known as Batten disease, comprise a group of rare inherited lysosomal storage disorders (LSDs) that predominantly affect the neurological systems of children.[1,2] CLN1 (neuronal ceroid lipofuscinosis type 1) is caused by bi-allelic loss-of-function mutations in the lysosomal enzyme palmitoyl-protein transferase 1 (PPT1) encoded by the *PPT1* gene.[3] PPT1 is a small glycoprotein that hydrolyzes the thioester bond linking long-chain fatty acids, such as palmitate, to cysteine residues of proteins. The removal of palmitate allows these proteins to be degraded by the lysosomal system. Defects in the PPT1 gene lead to CLN1 disease, also known as infantile neuronal ceroid lipofuscinosis type 1. CLN1 is characterized by accumulation of autofluorescent storage material (AFSM) and disruption of lysosomal function in the central nervous system (CNS). Non-dividing cells, such as neurons, are particularly vulnerable to this dysfunction, and CLN1 patients suffer from a diverse array of neurological symptoms including rapid motor and cognitive decline, vision loss, and premature death.[4,5]

The mainstay of treatment for many LSDs is enzyme replacement therapy (ERT).[6,7] It has shown clinical success in CLN2, where recurring intra-CNS deliveries of TPP1, an ERT branded as Brineura, helped children reach key milestones.[8,9] In CLN1, ERT halted disease progression in rodents and demonstrated partial preservation of brain morphology in *Ppt1*$^{-/-}$ sheep.[10] Blood brain barrier-penetrant ERT has also been used on a compassionate case in Germany.[11] However, significant dosing refinement and safety assessment in large animals is needed before clinical application. Furthermore, ERT requires lifelong repeated CNS infusions and may not address emerging systemic disease aspects.[12] As an alternative, adeno-associated virus

Received 4 April 2025; accepted 8 July 2025;
https://doi.org/10.1016/j.ymthe.2025.07.011.

Correspondence: Md Suhail Alam, Spark Therapeutics, Inc., 3025 Market Street, Philadelphia, PA 19104, USA.
E-mail: suhail.alam.sa1@roche.com
Correspondence: Maria Grazia Biferi, Spark Therapeutics, Inc., 3025 Market Street, Philadelphia, PA 19104, USA.
E-mail: maria.graziabiferi@sparktx.com

Please cite this article in press as: Alam et al., AAV-delivered PPT1 provides long-term neurological benefits in CLN1 mice and achieves therapeutic levels in sheep brain, Molecular Therapy (2025), https://doi.org/10.1016/j.ymthe.2025.07.011

(AAV)-vectorized PPT1 offers a potential long-term solution by enabling sustained therapeutic enzyme expression in the transduced cells, with the added benefit of cross-correction through enzyme secretion and uptake by neighboring cells.

AAV vector delivery directly into the brain parenchyma, or via intrathecal administration, or a combination of these approaches, has shown convincing benefits in a CLN1 mouse model.[13–15] Similar studies in rodents by Taysha Gene Therapies resulted in the intrathecal administration of a gene therapeutic to the first CLN1 patients in an investigator-initiated study.[16] However, CLN1 disease is characterized by widespread lysosomal dysfunction[14,17] and neurodegeneration,[14,18,19] requiring therapeutic levels of PPT1 throughout the CNS, including deep brain regions such as thalamus, brain stem, and cerebellum. Achieving widespread distribution of PPT1 in the CNS remains a significant hurdle, with intrathecal delivery leading to limited therapeutic benefits in the mouse model.[14] To address these issues, we designed and tested an AAV encoding a modified PPT1 transgene with enhanced cross-correction potential, utilizing a proprietary capsid, Spark100, that transduces neurons with high efficiency.

Herein we report a single intracerebroventricular (i.c.v.) delivery of single-stranded AAV-Spark100-PPT1 vector in the neonatal *Ppt1*$^{-/-}$ mouse model preserved neurobehavioral functions, prevented the buildup of lysosomal storage material, blocked neuroinflammation, and doubled the lifespan. PPT1 levels remained above therapeutic thresholds across the CNS in *Ppt1*$^{-/-}$ mice for up to 15 months. In a preliminary biodistribution study designed to model delivery route and pharmacodynamic effect, i.c.v. delivery of gene therapy vectors in adult *Ppt1*$^{+/-}$ sheep showed widespread PPT1 activity, exceeding predicted therapeutic levels throughout the brain, and was well tolerated. Together, these data suggest that Spark100. PPT1 has potential for further development as a treatment for CLN1 disease and that a similar AAV platform might be useful in the treatment of diverse conditions employing a secreted therapeutic transgene.

RESULTS

In vitro screening and identification of engineered PPT1 designs for enhanced cross-correction

AAV-based gene augmentation therapy for many LSDs provides the unique advantage of enhancing therapeutic efficacy through cross-correction.[20] To evaluate the potential for cross-correction to treat CLN1, we modified the signal peptide of human PPT1 to improve its secretion capacity. Nine heterologous signal peptides were evaluated against the native PPT1 signal peptide sequence (Table S1). Expression of secretable *PPT1* was mediated by the ubiquitous human eukaryotic translation elongation factor 1 alpha (EF1α) promoter and a polyadenylation (polyA) signal from the bovine growth hormone gene (Figure 1A). To correct for plasmid transfection efficiency and streamline uptake assay analysis, an additional expression cassette encoding TdTomato as a fluorescent reporter was incorporated into the backbone of plasmids used for *in vitro* screenings. The screening was conducted in a *PPT1*$^{-/-}$ human cell line along with *in silico* immunogenicity assessment and identified two lead transgene designs that we referred to as lead 1 and lead 2 (Figure 1B). Lead 1 contains the signal sequence from the human chymotrypsinogen B2 and in lead 2, the signal sequence is from the human SPARC gene (Figure 1C; Table S1).

Whereas intracellular pools of PPT1 were equivalent across all transgene designs, lead 1 and lead 2 increased the activity of PPT1 in cell culture supernatants by approximately 25%–50% compared with the native sequence (Figures 1D and 1E). Glycosylation of PPT1 is required for cellular uptake and cross-correction. In both designs, glycosylation of PPT1 appeared similar to that obtained using the native sequence (Figure S1). Quantitative immunofluorescence analysis showed a significantly higher number of PPT1-positive cells among non-transduced cells (TdTomato negative) in both lead 1 and lead 2 compared with the native PPT1, suggesting that cross-correction occurred in this cell culture model (Figures 1F and 1G). The signal sequence in lead 1, when fused to alpha-glucosidase for Pompe disease, raised no safety concerns in mouse and non-human primate (NHP) models.[21,22] Therefore, lead 1 was vectorized in AAV-Spark100 for further evaluation. AAV-Spark100 is an engineered capsid capable of transducing a wide variety of cell types in humans and non-clinical species. It has been used for both liver and brain-directed gene therapies that have advanced to human testing for hemophilia B[23] and Huntington's diseases.[24]

i.c.v.-delivered AAV.PPT1 vectors resulted in widespread vector distribution and transgene expression in WT mice

A pilot biodistribution study was conducted in wild-type (WT) mice to establish technical proof of concept. Single-stranded AAV vector carrying lead 1 was administered at two doses, 1×10^{10} vector genomes (vg) and 1×10^{11} vg per animal, *via* bilateral i.c.v. injection in postnatal day 1 (PND1) pups (Table S2). Six weeks post dosing, tissues were analyzed for vector genome distribution and PPT1 enzymatic activity (Figure S2A). No abnormal changes in body nor brain weight were observed (Figures S2B and S2C). Quantitative PCR showed dose-dependent vector genome distribution across brain regions and the spinal cord (Figure S2D), with corresponding increases in PPT1 enzymatic activity in brain regions and cerebrospinal fluid (CSF) (Figures S2E and S2F). Consistent with our *in vitro* results, overexpressed PPT1 in the mouse brain was glycosylated (Figure S2G). Increased PPT1 activity in brain correlated with vector genome copy number (VGCN) (Figure S2H). These findings demonstrated that i.c.v. delivery of lead 1 encoded secretable PPT1, supported widespread PPT1 expression in the CNS, and was well tolerated.

One-time i.c.v. delivery of PPT1 gene therapy prevented premature death of *Ppt1*$^{-/-}$ mice

The *Ppt1*$^{-/-}$ mouse model recapitulates key histopathological and behavioral characteristics of CLN1 disease[25] and has proven suitable for investigating gene therapy-based treatments.[13,14] To evaluate the efficacy of our gene therapy candidate in *Ppt1*$^{-/-}$ mice, we

Please cite this article in press as: Alam et al., AAV-delivered PPT1 provides long-term neurological benefits in CLN1 mice and achieves therapeutic levels in sheep brain, Molecular Therapy (2025), https://doi.org/10.1016/j.ymthe.2025.07.011

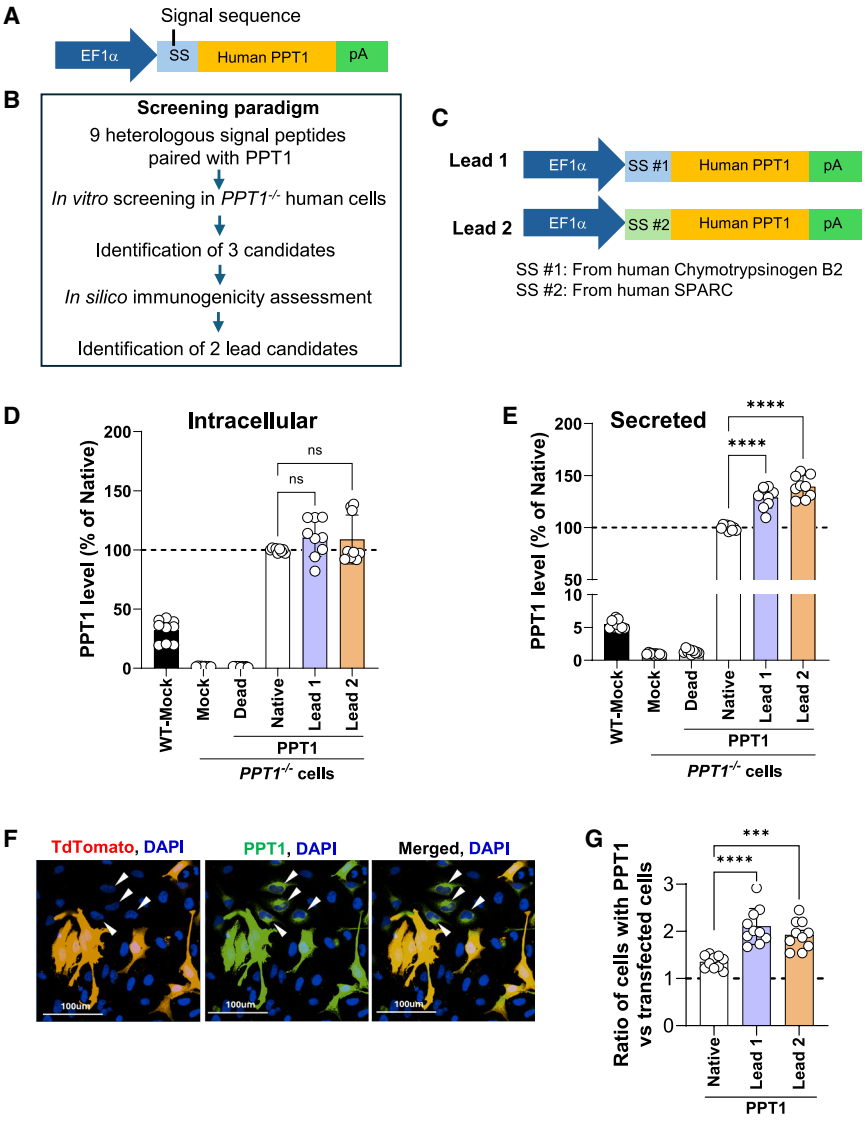

Figure 1. AAV.PPT1 construct expressing human *PPT1* and identification of two lead engineered PPT1 designs

(A) PPT1 expression cassette comprising the human EF1α promoter, signal sequence (SS) from human PPT1 or from highly secreted non-heterologous human proteins (as listed in Table S1) was paired with cDNA of human *PPT1* gene followed by polyadenylation (pA) sequence from bovine growth hormone (BGH). (B) Overall experimental paradigm for screening nine engineered PPT1 candidates using *in vitro* and *in silico* models resulting in the identification of two lead candidates. (C) Expression cassette designs for lead 1 and lead 2. (D and E) PPT1 activity in intracellular (D), and secreted fractions (E) from $PPT1^{-/-}$ cells transfected with AAV plasmids. Native (unmodified human PPT1), catalytically dead (PPT1 Ser115Ala, His289Ala), leads 1 and 2 were analyzed for PPT1 activity 48-h post-transfection. (F) Representative fluorescence micrographs detecting PPT1 (green) using anti-PPT1 antibodies, or TdTomato (red) directly in $PPT1^{-/-}$ cells transfected with lead 1. White arrowheads mark non-transfected (TdTomato-negative) cells that are PPT1-positive, indicating the uptake of secreted PPT1. DAPI-stained nuclei are shown in blue. (G) Ratio of PPT1-positive cells to TdTomato-positive cells. Higher ratios suggest higher PPT1 uptake. In (D), (E), and (G), each data point represents an independently transfected well. $n = 3$ independent experiments, each consisting of 3–4 transfected wells. The values are mean (SD). One-way ANOVA with Dunnett's test comparing lead 1 and lead 2 with native. ns, non-significant; $^{***}p < 0.001$, $^{****}p < 0.0001$.

administered two doses (low, 1×10^{11} vg; high, 3.82×10^{11} vg per animal) of lead 1 via bilateral i.c.v. injection at PND 1–3 (Figure 2A) and mice were longitudinally assessed up to 15 months. Unmodified PPT1 referred to as "native" was tested at both doses as a control and reference. Diluent-injected and un-injected mice served as additional control groups (Table S3). Neurobehavioral assessments commenced at 5 months of age, at which time animals are largely asymptomatic,[14] and were performed longitudinally at intervals of 2–3 months until 14 months of age (Figure 2A). Histopathological analysis was performed on a subset of 8- to 10-month-old animals, which is considered end stage of disease in this model (Figure 2A).

Serum analysis at 1 month confirmed the expression of secreted PPT1 in treated animals (Figure S3), with the high-dose lead 1 group exhibiting an ~85% greater increase ($p < 0.001$) compared with the dose-matched native group. Consistent with previous studies,[25,26] the median survival for untreated $Ppt1^{-/-}$ mice, or controls, was 38 and 36 weeks, respectively (Figure 2B). In contrast, most gene therapy-treated $Ppt1^{-/-}$ mice survived until the study's pre-defined endpoint at 65 weeks (15 months), except a few random mortality events (1 or 2 animals per cohort) (Figure 2B). As expected, statistical analysis of lifespan showed that all pairwise comparisons from treatment groups (and WT) are significantly different compared with the untreated and diluent-injected controls, and no differences were detected between the treated cohorts and WT controls. Maximum survival efficacy was achieved even with the low dose of AAV for both native PPT1 and lead 1 (Figure 2B).

i.c.v.-delivered PPT1 gene therapy provided long-term preservation of motor function, grip strength, and gait in $Ppt1^{-/-}$ mice

$Ppt1^{-/-}$ mice exhibit motor and gait deficits that mirror key neurobehavioral symptoms in CLN1 patients. Therefore, motor function assessments were conducted starting at 5 months (asymptomatic) of age, with grip tests and gait analysis added later (Figure 2A).

Please cite this article in press as: Alam et al., AAV-delivered PPT1 provides long-term neurological benefits in CLN1 mice and achieves therapeutic levels in sheep brain, Molecular Therapy (2025), https://doi.org/10.1016/j.ymthe.2025.07.011

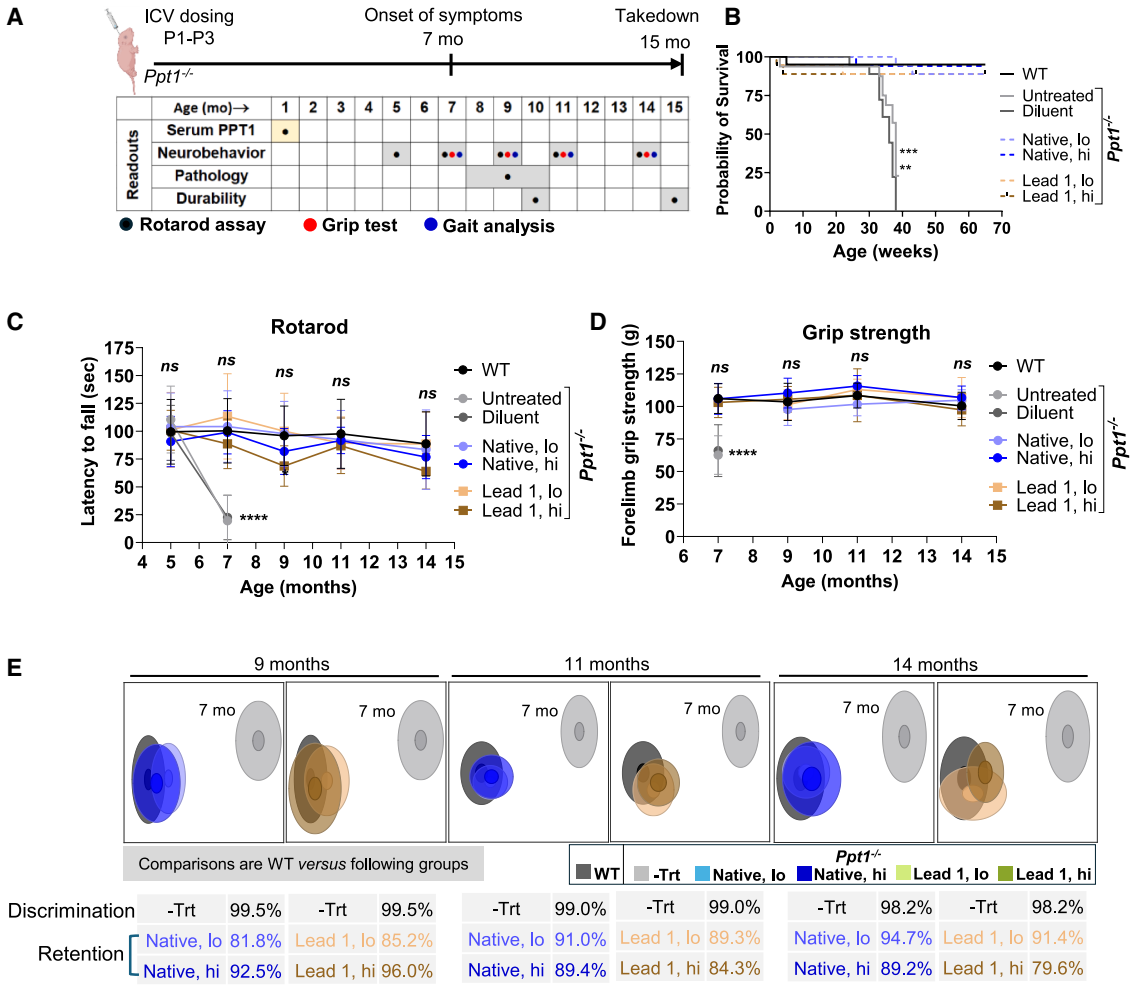

Figure 2. Neonatal i.c.v. administration of AAV.PPT1 gene therapy extended survival and provided long-term preservation of neurobehavioral functions in *Ppt1*$^{-/-}$ mice

(A) Study design outlines the study readouts and data collection time course. Two doses: (1) low (lo), 1×10^{11} vg/animal and (2) high (hi), 3.82×10^{11} vg/animal of AAV vectors carrying unmodified PPT1 (native) or lead 1 were administered by bilateral i.c.v. route at P1–P3. In each group, 16–20 animals, proportionally balanced for gender, were enrolled. Tissues were collected at 8–10 months from four to six animals per group for neuropathology and durability assessments, except for the lead 1, hi group, which included nine animals. (B) Kaplan-Meier survival analysis curves showing survival benefit of gene therapy in *Ppt1*$^{-/-}$ mice. Pairwise comparisons with Benjamini-Hochberg correction demonstrated untreated and diluent-treated *Ppt1*$^{-/-}$ group significantly differed from WT (***$p < 0.001$) and with gene therapy-treated animals (**$p < 0.01$). No significant difference in survival was observed between gene therapy-treated *Ppt1*$^{-/-}$ animals and WT mice. Number of animals in the groups from top to bottom were 20, 16, 18, 18, 17, 18, and 18. (C) Accelerating rotarod showed untreated or diluent-treated *Ppt1*$^{-/-}$ mice fell over faster at 7 months (****$p < 0.0001$), while gene therapy-treated *Ppt1*$^{-/-}$ mice showed no significant difference (p = ns) compared with WT at all ages, except for a minor transient decline (*$p < 0.05$) in lead 1, hi at 9 months compared with WT or lead 1, lo. N = 14–19/group (from 5 to 7 months) and N = 10–18/group (from 9 to 14 months) except lead 1, hi group where N = 7. (D) The grip strength test showed significantly weaker forelimb strength (****$p < 0.0001$) in untreated or diluent-treated *Ppt1*$^{-/-}$ mice vs. WT at 7 months. Gene therapy-treated animals showed no significant difference (p = ns) from age-matched WT mice at all ages. (E) De-correlated ranked feature-based cloud analysis of NeuroCube results detected gait changes in control and gene therapy-treated *Ppt1*$^{-/-}$ mice at indicated time points. "Percentage discrimination" shows the degree by which the cumulative gait parameters of control *Ppt1*$^{-/-}$ mice (untreated and diluent-treated combined and referred to as -Trt) differed from WT animals, while "percentage retention" indicates the overlap in the gait features of gene therapy-treated groups to WT animals. As untreated *Ppt1*$^{-/-}$ mice did not survive beyond 8 months, data from 7-month-old control *Ppt1*$^{-/-}$ animals (-Trt), were compared with WT mice across the 9- to 14-month time points. In (D) and (E), N = 7–16/group (at 7 months) and N = 10–18/group (from 9 to 14 months) except lead 1, hi group where N = 7. lo, low dose, 1×10^{11} vg/animal; hi, high dose, 3.82×10^{11} vg/animal. In (C) and (D), data are presented as mean (SD). A 1-way ANOVA with Tukey's test for multiple comparisons between the groups at each time point. In (C) and (D), *$p < 0.05$, lead 1, hi vs. either WT or lead 1, lo at 9 months of age; ****$p < 0.0001$, *Ppt1*$^{-/-}$, untreated or diluent vs. WT at 7 months.

Please cite this article in press as: Alam et al., AAV-delivered PPT1 provides long-term neurological benefits in CLN1 mice and achieves therapeutic levels in sheep brain, Molecular Therapy (2025), https://doi.org/10.1016/j.ymthe.2025.07.011

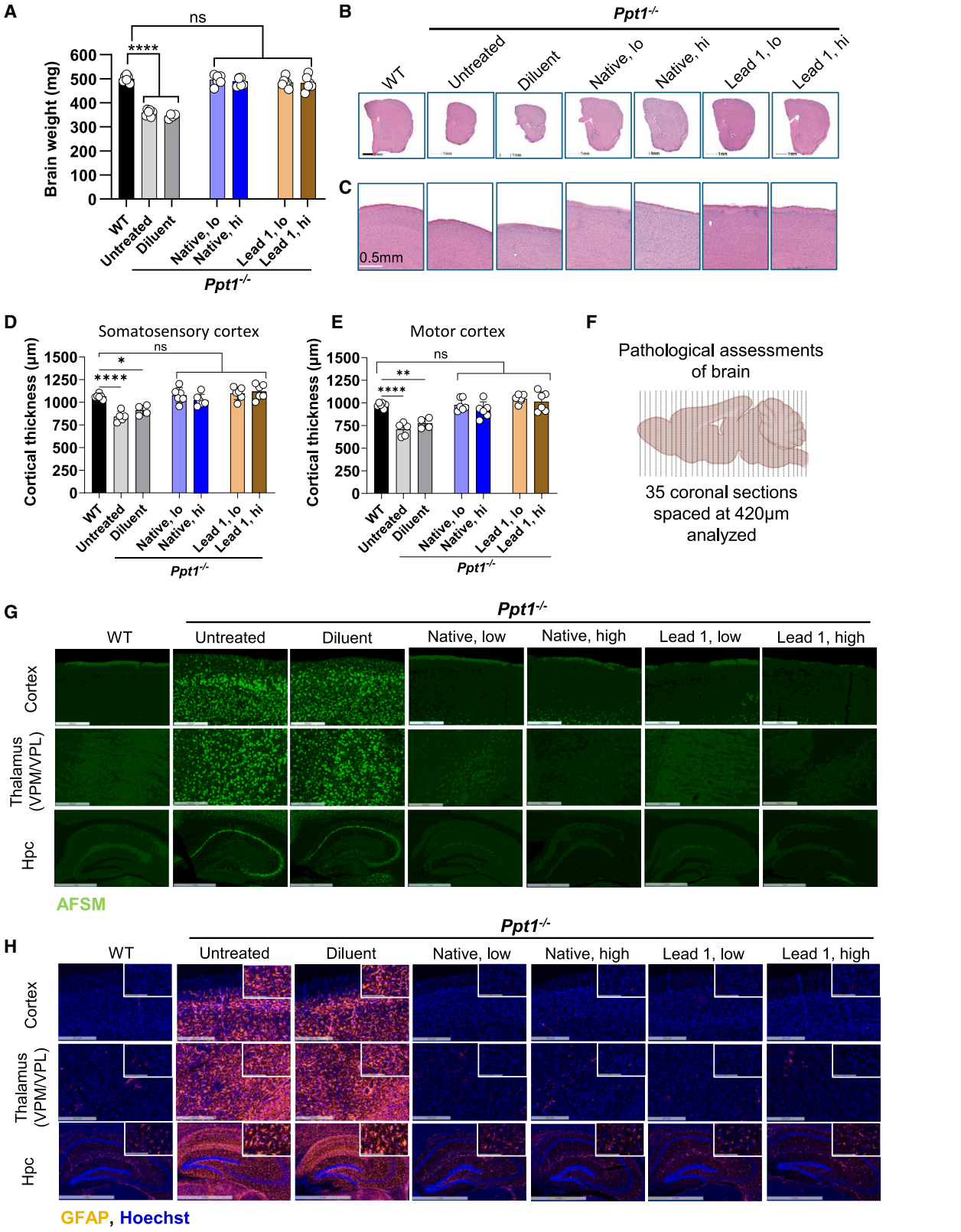

(legend on next page)

Please cite this article in press as: Alam et al., AAV-delivered PPT1 provides long-term neurological benefits in CLN1 mice and achieves therapeutic levels in sheep brain, Molecular Therapy (2025), https://doi.org/10.1016/j.ymthe.2025.07.011

The accelerated rotarod assessment showed significant deterioration of motor function in *Ppt1*$^{-/-}$ mice at 7 months, whereas it was completely rescued in treated animals (Figure 2C). Consistent with survival studies, gene therapy treatment resulted in a full rescue of rotarod dysfunction, regardless of dose or transgene design (Figure 2C).

While motor function impairment is well established in both clinical cases and mouse models of CLN1 disease, the impact on muscular strength remains unclear. We hypothesized that, akin to some other LSDs,[27] CLN1 might also impact muscle function. Indeed, we observed a significant ∼40% reduction ($p < 0.0001$) in forelimb grip strength in *Ppt1*$^{-/-}$ mice at 7 months of age, the earliest age at which mice were assessed (Figure 2D). Similar to the rotarod results, forelimb grip strength was fully preserved in all treated groups, mirroring that of WT mice throughout the study duration (Figure 2D).

Gait was analyzed using NeuroCube,[28] a behavioral platform with automated video capture and analysis to investigate changes in gait geometry and dynamics in rodent models. De-correlated ranked feature-based cloud analysis of over 100 gait parameters showed that *Ppt1*$^{-/-}$ mice at 7 months of age exhibited notable altered gait features compared with WT mice (Figure 2E). In contrast, gene therapy-treated *Ppt1*$^{-/-}$ mice exhibited notable gait feature similarities (referred to as retention) to WT animals at all ages. At 9 months of age, the native PPT1-treated cohort showed 82% retention in the low-dose group and 92% in the high-dose group compared with age-matched WT mice. Mice treated with lead 1 showed 85% and 96% retention of gait features in the low- and high-dose groups, respectively (Figure 2E). Both the native and lead 1 groups maintained substantial retention of gait features at both dose levels, achieving over 91%–94% retention in the low-dose groups and 80%–89% retention in the high-dose groups at 14 months of age (Figure 2E).

PPT1 gene therapy provided long-term sustained protection from brain atrophy in the *Ppt1*$^{-/-}$ mice

Brain atrophy is reported in CLN1 patients,[3] CLN1 mouse models,[29] and in a PPT1-deficient sheep model.[30] Brain weight and cortical thickness were measured to evaluate the effect of treatment on brain atrophy. Consistent with earlier findings,[29] we found a significant ∼30% reduction ($p < 0.0001$) in brain weight in untreated *Ppt1*$^{-/-}$ mice compared with WT mice at 8–10 months of age (Figure 3A). In contrast, brain weights of gene therapy-treated mice showed no significant difference from age-matched WT controls demonstrating that the treatment fully preserved the brain mass (Figure 3A). Assessment of H&E-stained coronal sections (at three consistent coronal planes) further confirmed reduced brain size in untreated mice, while treatment prevented global brain atrophy (Figure 3B). The quantitative analysis of cortical thickness in the motor and somatosensory regions aligned with the overall brain atrophy, showing mean reductions of 22% and 25%, respectively, in untreated *Ppt1*$^{-/-}$ mice (Figures 3D and 3E). In contrast, gene therapy-treated mice maintained cortical thickness similar to WT in both regions (Figures 3D and 3E).

PPT1 gene therapy prevented the accumulation of AFSM and blocked neuroinflammation in the brain of CLN1 mice

In CLN1 disease, AFSM accumulation in the CNS starts early and, in mouse models, is linked to progressive neuronal loss and the worsening of patient-relevant neurobehavioral outcomes.[31] To assess the effect on AFSM, we conducted a comprehensive analysis across the entire brain of 8- to 10-month-old mice, analyzing 35 equally spaced coronal sections covering the full hemisphere (Figure 3F). The images in Figure 3G represent the cortex, thalamus (VPM/VPL regions), and hippocampus, showing substantial AFSM accumulation in these areas in untreated or diluent-treated end-stage *Ppt1*$^{-/-}$ mice. Remarkably, mice treated with gene therapy vectors, regardless of candidate or dose, displayed minimal to no AFSM in all three brain regions (Figure 3G). Similar results were observed throughout other brain areas.

Neuroinflammation is a prominent pathological feature in the CLN1 mouse model, characterized by extensive astrocyte activation and their proliferation, which increases as the disease progresses, correlating closely with neurodegeneration.[18,32] Neuroinflammation may significantly contribute to disease pathology, intensifying neuronal loss and motor impairment. The representative micrographs presented in Figure 3H demonstrate widespread brain astrocytosis in cortex, thalamus, and hippocampus of untreated or diluent-treated *Ppt1*$^{-/-}$ mice. The brains of gene therapy-treated mice were remarkably similar to those of WT animals (Figure 3H), suggesting that astrocytosis was completely prevented. This result

Figure 3. PPT1 gene therapy prevented brain atrophy, buildup of storage material, and astrocytosis across brain regions in *Ppt1*$^{-/-}$ mice at 8–10 months of age

(A) Brain weight of indicated groups. (B) Representative H&E-stained coronal sections of brain hemisphere. Three sections from consistent planes in each animal were analyzed. Scale bar, 1 mm. (C) Representative H&E-stained images of coronal hemi brain sections showing reduced cortical thickness in untreated and diluent-treated *Ppt1*$^{-/-}$ mice while gene therapy treatment prevented cortical thinning. Scale bar, 0.5 mm. (D and E) Quantification of cortical thickness from somatosensory (D) and motor cortex (E) regions. Each circle represents mean of three sections spaced at 840 μm from each animal. (F) Thirty-five coronal sections, 420 μm apart, spanning the entire brain hemisphere were analyzed for AFSM and astrocytosis using fluorescence microcopy and representative images are presented in (G) and (H). (G) Micrographs detecting AFSM (green puncta) and (H) astrocytes (red) in the cortex, thalamus (VPM/VPL), and hippocampus (Hpc). Insets are the magnified regions from the corresponding brain regions. In (G), the scale bar is 250 μm for cortex and thalamus and 1 mm for the hippocampus. In (H), it is 200 μm for cortex and thalamus, 1 mm for the hippocampus, and 100 μm for insets. lo, low dose, 1×10^{11} vg/animal; hi, high dose, 3.82×10^{11} vg/animal. Quantitative data and representative images are from gender-balanced groups of $N = 4$–6/group. In (A), (D), and (E), data are mean (SD). One-way ANOVA, Tukey's post hoc test. *$p < 0.05$, **$p < 0.01$, ****$p < 0.0001$.

Please cite this article in press as: Alam et al., AAV-delivered PPT1 provides long-term neurological benefits in CLN1 mice and achieves therapeutic levels in sheep brain, Molecular Therapy (2025), https://doi.org/10.1016/j.ymthe.2025.07.011

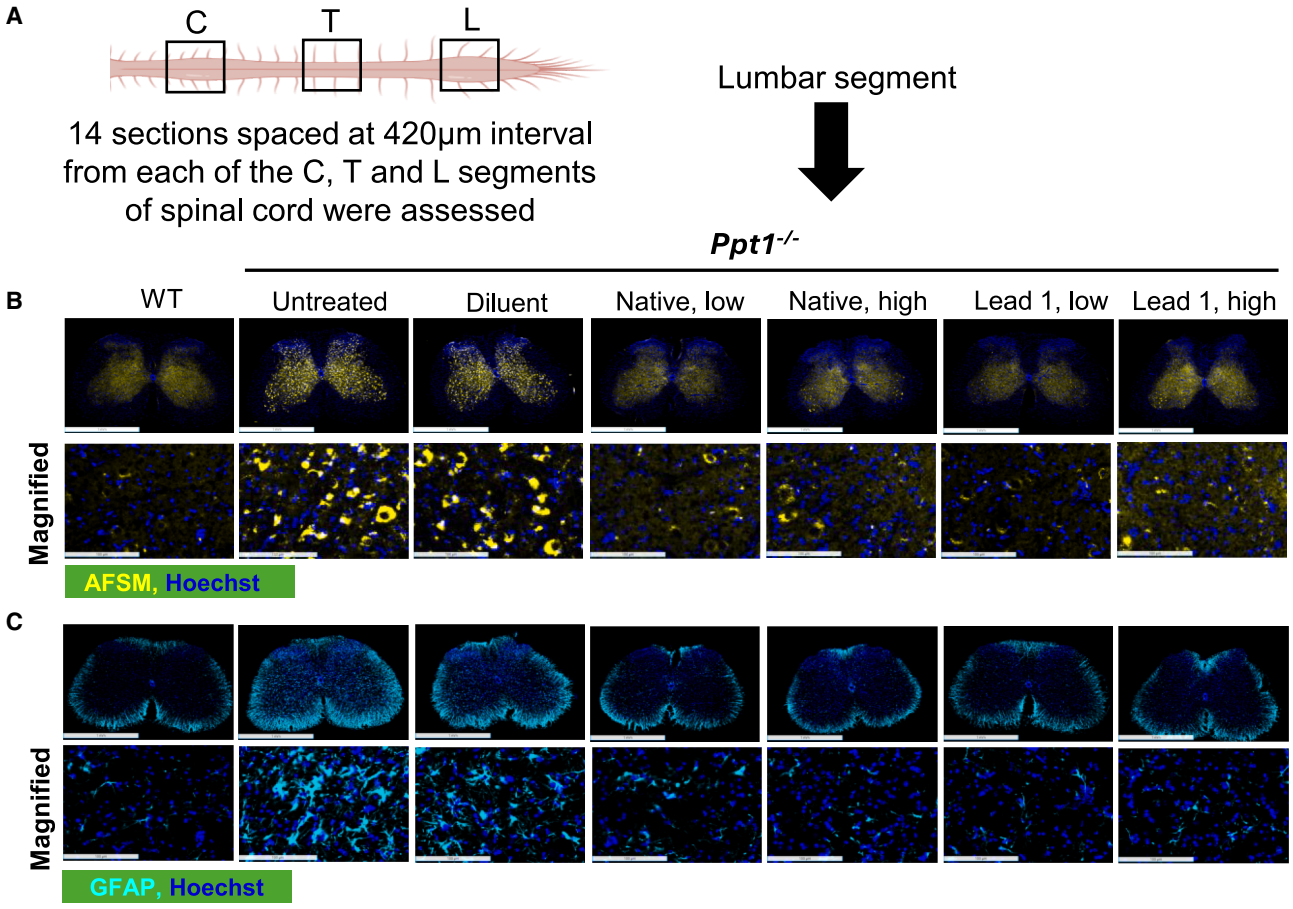

Figure 4. Gene therapy prevented accumulation of storage materials and blocked astrocytosis in the spinal cord of *Ppt1*$^{-/-}$ mice at 8–10 months of age

(A) Fourteen transverse sections from the cervical (C), thoracic (T), and lumbar (L) segments from mice (N = 4–6/group, gender balanced) were analyzed for AFSM and astrocytosis. Images from the lumbar segment are shown in (B) and (C). (B) Fluorescence microscopy detecting autofluorescence storage signal (pseudo-colored and shown in yellow) close to nuclei (blue). (C) Sections stained with anti-GFAP antibodies showing labeling of astrocytes (cyan). Images in (B) and (C) are representative. Nuclei stained with Hoechst are shown in blue. The scale bar for the top row images in (B) and (C) is 1 mm, while for the magnified images, it is 100 μm. GFAP, glial fibrillary acidic protein. Low dose, 1×10^{11} vg/animal; high dose, 3.82×10^{11} vg/animal.

aligns well with the observed protective outcomes on motor function (Figure 2C), muscle strength (Figure 2D), gait (Figure 2E), and the prevention of brain mass loss and cortical atrophy (Figures 3A–3E).

PPT1 gene therapy prevented AFSM accumulation and neuroinflammation in the spinal cord of *Ppt1*$^{-/-}$ mice

As in the brain, neuropathological features are also prominent in the spinal cord.[14] To assess whether PPT1 gene therapy benefited the spinal cord, 14 transverse sections from each of the cervical, thoracic, and lumbar regions were analyzed for AFSM and astrocytosis (Figure 4A). Fluorescence micrographs of lumbar segment shown in Figure 4B demonstrated buildup of storage material and markedly enhanced activation and proliferation of astrocytes (Figure 4C) in the untreated *Ppt1*$^{-/-}$ mice. Similar to the findings in brain, both pathological makers were markedly reduced in the spinal cord of CLN1 mice treated with gene therapy (Figures 4B and 4C). Results were similar in cervical and thoracic segments (Figure S4).

Gene therapy demonstrated durable and sustained long-term expression of PPT1 in the CNS without inducing any adverse effects in the CLN1 mice

Previous studies have tested intrathecal-delivered AAV-based gene therapy in neonatal *Ppt1*$^{-/-}$ mice, but the long-term persistence and functionality of the vector for sustained PPT1 expression was not evaluated.[13,14] In this study, we assessed the durability of the vector and its ability to support active PPT1 expression over an extended period from 10 to 15 months of age (Figure 5A). Vector genome analysis at 10 months in lead 1-dosed animals showed a dose-dependent distribution of vector DNA across key CNS regions, with the highest levels in the cortex (Figure 5B). Correspondingly, activity assays revealed dose-dependent, supraphysiological PPT1 expression

Please cite this article in press as: Alam et al., AAV-delivered PPT1 provides long-term neurological benefits in CLN1 mice and achieves therapeutic levels in sheep brain, Molecular Therapy (2025), https://doi.org/10.1016/j.ymthe.2025.07.011

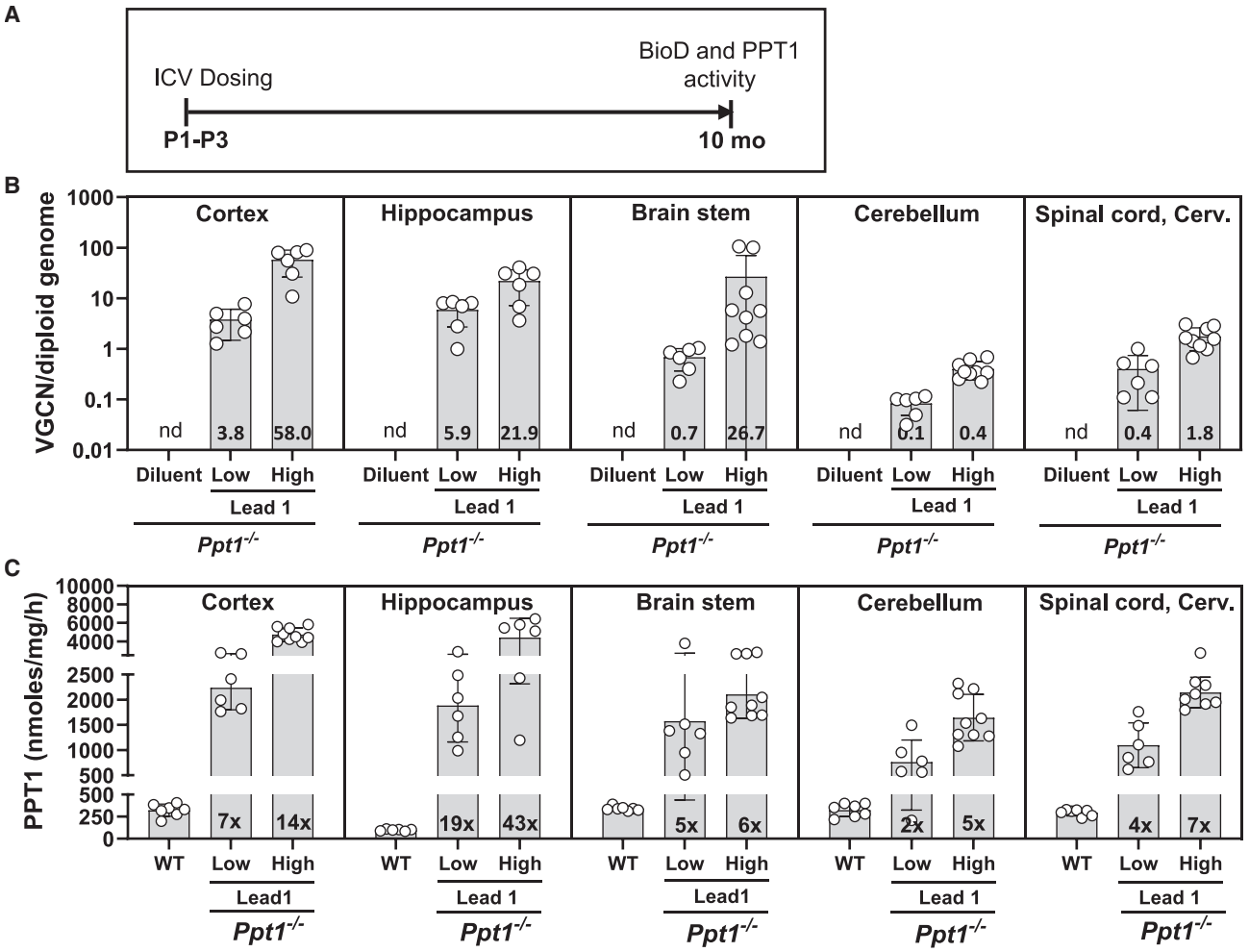

Figure 5. Long-term vector persistence and PPT1 expression in the brain and spinal cord of *Ppt1*$^{-/-}$ mice 10 months post dosing

(A) Two doses of lead 1 (low, 1 × 10^{11} vg/animal and high, 3.82 × 10^{11} vg/animal) were administered via i.c.v. to *Ppt1*$^{-/-}$ mice at P1–P3. VGCN and PPT1 activity were quantified at 10 months. (B) Quantification of VGCN by TaqMan qPCR showing dose-dependent presence of vector DNA. The VGCN are shown per diploid genome of host cell in the indicated CNS regions. (C) PPT1 activity in the indicated CNS regions of *Ppt1*$^{-/-}$ mice. The numbers within the bars are the fold increases in the mean VGCN or PPT1 activity in the gene therapy-dosed mice compared with the mean VGCN and PPT1 activity of WT mice. *N* = 6–9 per group except diluent where *N* = 4, gender proportionally balanced. Data in both panels are mean (SD). nd, not detected.

throughout the CNS (Figures 5C and S5), including typically hard-to-access subcortical regions such as the thalamus, brainstem, and cerebellum, where PPT1 activity increased 17-, 6-, and 5-fold, respectively, in the high-dose group compared with WT mice.

For gaining deeper insights and spatial context, we performed immunohistochemical (IHC) analysis of 35 coronal brain sections covering the entire brain from rostral to caudal axis at 8–10 months of age. Representative images from eight evenly spaced coronal sections (Figures 6A and 6B) highlighted robust PPT1 signals across cortical structures, thalamus, and the hippocampus, aligning with the elevated PPT1 activity data presented in Figure 5B. In the spinal cord, PPT1 staining was predominantly localized in the gray matter, with an intense signal in the ventral horns of all three segments (Figure 6C). Morphological assessment showed that PPT1 was highly expressed within the larger neurons, which are likely motor neurons (Figure 6C, magnified 1, indicated by white arrowheads). Based on the punctate and perinuclear signal, we inferred that PPT1 may be localized within the lysosomes (Figure 6C, magnified 2, indicated by orange arrowheads); however, co-localization assessment with a lysosomal marker is required for validation. These findings suggested that a single, early-life i.c.v. dose of PPT1 gene therapy can achieve long-lasting, widespread therapeutic PPT1 expression not only in the brain but also in the spinal cord of CLN1 mice, signifying that the technology provides global CNS correction of the disease phenotype. Further evaluation of the brain and spinal cord at 15 months post-treatment revealed minimal to no decline in PPT1 activity levels (Figure S6), reinforcing the therapy's long-term durability.

Please cite this article in press as: Alam et al., AAV-delivered PPT1 provides long-term neurological benefits in CLN1 mice and achieves therapeutic levels in sheep brain, Molecular Therapy (2025), https://doi.org/10.1016/j.ymthe.2025.07.011

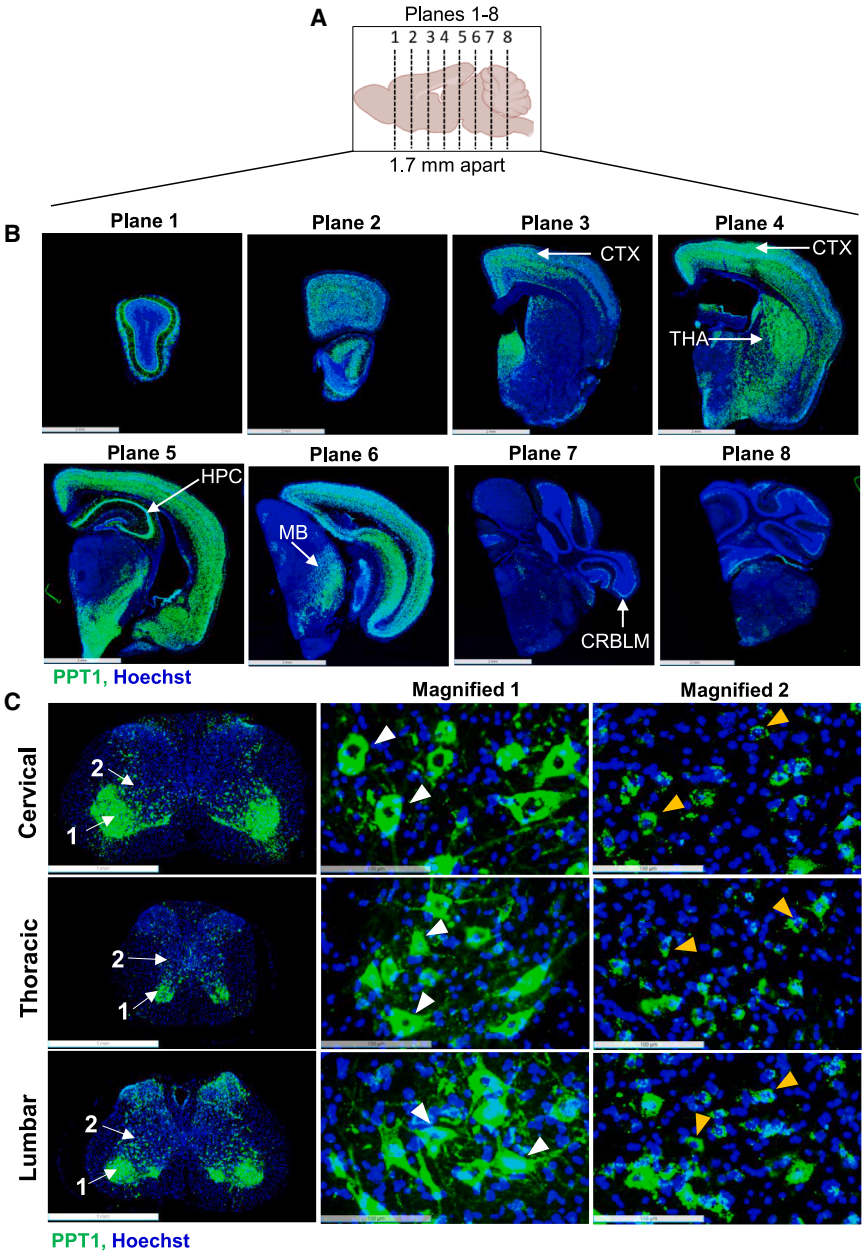

Figure 6. Indirect immunofluorescence analysis showed durable and widespread PPT1 expression in multiple brain regions and spinal cord of *Ppt1*$^{-/-}$ mice 10 months post dosing

The brain and spinal cord of *Ppt1*$^{-/-}$ mice treated with a high dose of lead 1 (3.82×10^{11} vg/animal) were collected 10 months post-treatment and PPT1 was detected by immunostaining. (A) Eight coronal sections of brain hemisphere spaced at 1.7 mm as shown by black dotted lines were stained with anti-PPT1 antibodies. (B) Images highlight PPT1 staining (green) in multiple brain areas. Prominent signal was noted in the cortex (CTX), hippocampus (HPC), thalamus (THA), and midbrain (MB). PPT1 signal was also observed in the cerebellum (CRBLM). Scale bar, 2 mm. (C) PPT1 (green) in the spinal cord was concentrated in the gray matter, with strong signals in the ventral horns. The area indicated by white arrows signifies magnified regions 1 and 2. The white arrowheads (magnified 1) indicate PPT1 expression in larger cells, likely motor neurons, while the orange arrowheads (magnified 2) point to the PPT1 signal surrounding the nuclei (blue) and are possibly within the lysosomes. Scale bar, 1 mm and in the magnified panels, 0.1 mm. Nuclei (blue) were stained with Hoechst. Images in (B) and (C) are representative of $N = 6$ (three females, three males).

In addition, treated groups showed strong long-term tolerance to the therapy, with no mortality aside from 1 to 2 early deaths/group, which was also observed in the untreated WT cohort (Figure 2B), no weight loss (Figure S7A), no loss of brain mass even at 15 months (Figure S7B), and no abnormal behavioral phenotypes observed. Even with sustained supraphysiological PPT1 levels in the CNS (up to 43-fold higher than the WT), no adverse findings were present highlighting the therapy was favorably tolerated in diseased animals.

Heterozygous human carriers[33] and animal models with one functional PPT1 allele[30,34] maintain about 50% of wild-type PPT1 levels and manifest no CLN1 disease, suggesting that restoring enzymatic activity to this threshold could significantly halt or slow CLN1 disease progression. The pharmacokinetic evaluation showed that in most of the areas even the low dose of both native and lead 1 resulted in PPT1 activity levels exceeding WT by more than 3-fold (Figure 5B showing lead 1; Figure S8 showing native). These levels significantly surpassed the targeted 50% PPT1 activity. The supraphysiological overexpression likely accounts for the full and saturated efficacies on lifespan, behavior, and neuropathology by the low-dose treatments for both native PPT1 and lead 1. A cumulative analysis across various CNS regions revealed that lead 1 induced up to 69% higher PPT1 activity ($p < 0.001$) in the CNS compared with the dose-matched group injected with native PPT1 (Figure S9A). The increased activity was likely attributable to enhanced secretion and subsequent uptake, since vector copy numbers were comparable between both candidates (Figure S9B).

i.c.v.-delivered PPT1 gene therapy showed broad vector distribution and elevated PPT1 activity in the CNS and was well tolerated in healthy sheep

Mouse models are vital for proof-of-concept studies. However, larger intermediate animal models are a key step in a preclinical evaluation

Please cite this article in press as: Alam et al., AAV-delivered PPT1 provides long-term neurological benefits in CLN1 mice and achieves therapeutic levels in sheep brain, Molecular Therapy (2025), https://doi.org/10.1016/j.ymthe.2025.07.011

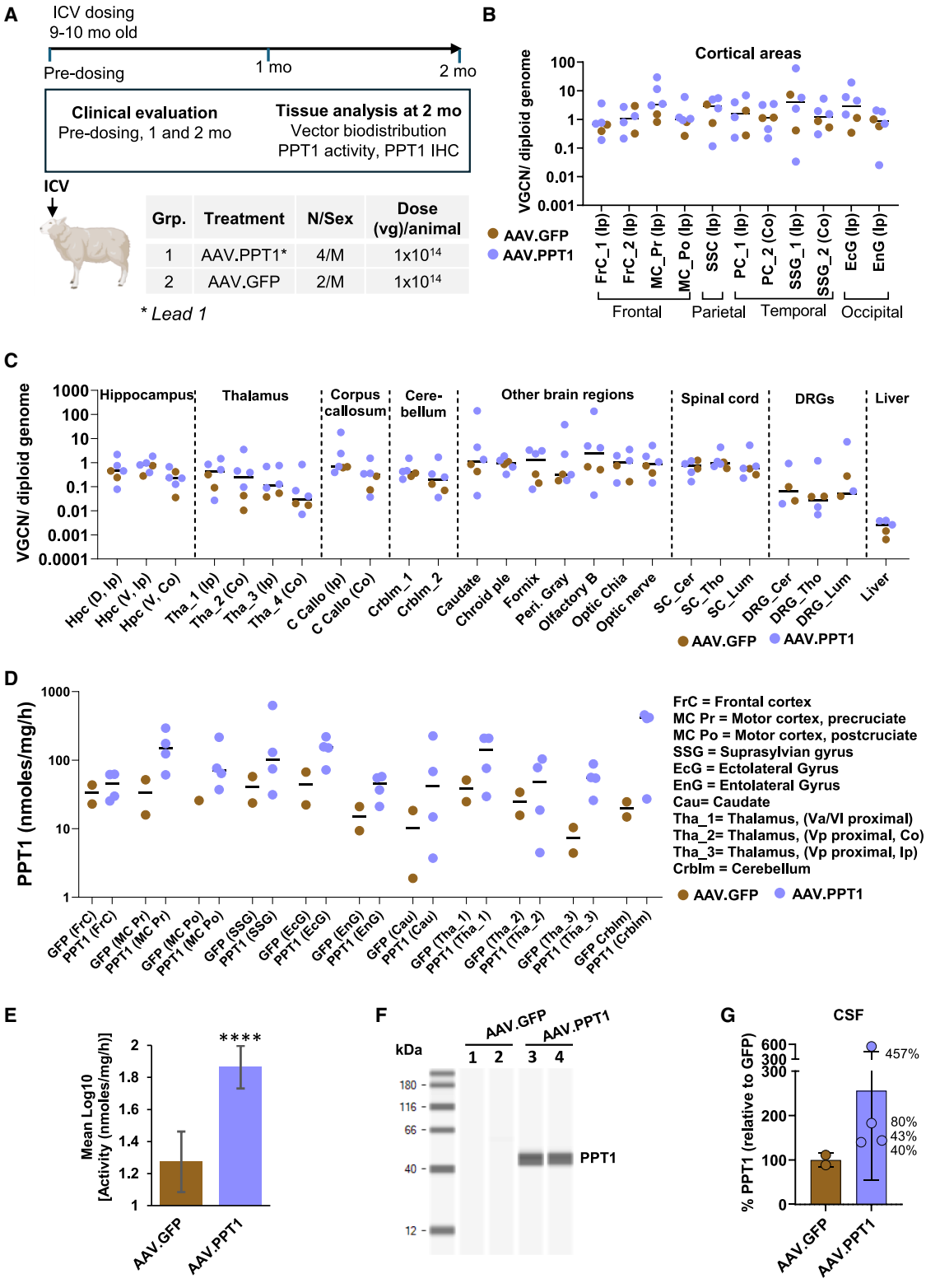

(legend on next page)

Please cite this article in press as: Alam et al., AAV-delivered PPT1 provides long-term neurological benefits in CLN1 mice and achieves therapeutic levels in sheep brain, Molecular Therapy (2025), https://doi.org/10.1016/j.ymthe.2025.07.011

by closely reflecting human CNS size and architecture, and supporting clinically relevant delivery modeling, biodistribution, and safety.[35–37] A large animal model greatly increases the likelihood of bridging the translational gap between rodent therapeutics and the clinical consideration for all the factors mentioned above. The CLN2 canine model enabled ERT approval,[38] while the CLN5 sheep model supported AAV gene therapy trials.[39–41] The CLN1 sheep model exhibits human disease-relevant features and responds to ERT.[10,30] Therefore, to further investigate the biodistribution and safety of PPT1 gene therapy, a preliminary non-good laboratory practice (GLP) study was conducted in healthy *Ppt1*$^{+/-}$ sheep in which PPT1 expression is approximately 50% lower than in WT animals.[10] The use of heterozygous animals typically presents an advantage over WT animals in overexpression studies, where transgene may reach supraphysiological levels of expression.

A 2-month study was conducted in 9- to 10-month-old sheep, where 1×10^{14} vg of lead 1 was administered via unilateral i.c.v. delivery to four animals, and two control animals received the same dose of an AAV expressing GFP (Figure 7A). The GFP vector group was used as a control to evaluate specific changes in PPT1 activity by the human *PPT1* transgene and to account for any effects on PPT1 expression or safety parameters resulting from the AAV capsid or the surgical procedure. Vector genome analysis of tissue punches collected at necropsy showed widespread vector distribution throughout the CNS. Brain region-specific analyses showed that within cortical regions covering all four cerebral lobes, the median VGCN ranged consistently between 0.6 and 4 vg/diploid genome (dg) (25th to 75th percentile ranged 0.3–5 vg/cell) (Figure 7B). Further exploration of pertinent brain areas included the thalamus, cerebellum, and hippocampus, alongside additional regions such as the corpus callosum, caudate, choroid plexus, fornix, and olfactory bulb. In the majority of these regions, the median VGCN consistently fell within the range of 0.3–0.9 vg/dg (Figure 7C). Additionally, an analysis of two vision-related regions, the optic chiasm and the optic nerve, showed a median vector load of 0.9 vg/dg) (Figure 7C). Notably, the data also revealed only slightly reduced vector distribution to the contralateral brain regions (annotated as "co" in parentheses in *x* axis labels of Figures 7B and 7C). All three segments of spinal cord (cervical, thoracic, and lumbar) also showed substantial vector distribution with the median values ranging between 0.5 and 0.9 vg/dg (Figure 7C). The median vector load in dorsal root ganglia (DRGs) ranged between 0.02 and 0.06 vg/dg, approximately 17-fold lower than the spinal cord regions (Figure 7C). Intra-CSF delivery of AAV vectors often results in significant peripheral leakage, leading to high liver transduction in rodents and NHPs.[42,43] Interestingly, the median vector load in the sheep liver was only 0.002 vg/dg (Figure 7C). The lower liver transduction could not be attributed to neutralizing antibodies to AAV-Spark100 capsid, as their pre-dosing blood titers were negligible (Table S4). Instead, the reduced vector load is likely due to either (1) minimal vector leakage into peripheral circulation or (2) the sheep liver being non-receptive to the AAV capsid used here.

Enzymatic assessment of PPT1 expression showed notable increases in multiple regions including various cortical structures, thalamus, caudate, and cerebellum compared with GFP animals (Figure 7D). Employing a combined analysis that considered both the number of tissue punches and potential variations in average values among brain regions, a hypothesis test confirmed an estimated 3.9-fold higher ($p < 0.0001$) PPT1 activity in the PPT1-dosed sheep relative to the GFP controls (Figure 7E). Automated western analysis confirmed that the PPT1 transgene product was intact, with no evidence of truncation (Figure 7F). Elevated PPT1 enzymatic activity was observed in the CSF, with PPT1-dosed animals showing increases ranging from 40% to 457% compared with GFP controls (Figure 7G). Consistent with our biochemical findings, immunofluorescence also revealed widespread and enhanced transgene expression, particularly in cortical structures and the cerebellum (Figures 8 and S10). While at lower levels, appreciable PPT1 expression was also detected in the caudate, thalamus, and brain stem (Figure S10). In GFP-dosed control animals, the antibody detected no reactivity (Figure S11). This could be due to PPT1 levels in heterozygous sheep being below the detection limit, or the antibody's exclusive specificity for human PPT1.

Figure 7. i.c.v. delivery of PPT1 gene therapy vectors and analysis of vector distribution and PPT1 expression in sheep

(A) Experimental design of a 2-month study to evaluate biodistribution and tolerability in sheep. PPT1 gene therapy vector (lead 1 referred as AAV.PPT1) or the Spark100 vector carrying GFP (AAV.GFP) was administered through unilateral i.c.v. route of delivery in 9- to 10-month-old healthy *Ppt1* heterozygous (*Ppt1*$^{+/-}$) males. Details of the dose, animal group sizes, and study readouts are listed. (B and C) qPCR results show VGCN per diploid genome (d.g.) in different CNS regions, as indicated. Frontal, parietal, temporal and occipital are the four lobes of brain. The horizontal bars indicate group median. (D) Results of PPT1 protein activity in brain regions as an index of PPT1 protein expression. The horizontal bars show group median. (E) Mean PPT1 activity in the sheep dosed with AAV.PPT1 was elevated by an estimated 3.9-fold compared with sheep dosed with AAV.GFP. Error bars show 95% confidence intervals. ****$p < 0.0001$, weighted two-way ANOVA. (F) Protein lysate from cerebellar punches of two control (AAV.GFP, lanes 1 and 2) and two AAV.PPT1-treated sheep (lanes 3 and 4) were analyzed using JESS. An intact PPT1 band at ~47 kDa was detected in samples from sheep dosed with the PPT1 vector. Lane 1, Molecular weight standards. kDa = kilodalton. (G) Elevated PPT1 activity in the CSF in AAV.PPT1-dosed animals. The percent change is relative to mean activity of GFP control. Each circle in (B–D), and (G) is an individual sheep. In (B) and (C), green spheres denote AAV.GFP samples, while blue spheres represent AAV.PPT1 samples. Numbers 1 and 2 after brain region abbreviations indicate punch samples from the same area. C Callo, corpus callosum; Cau, caudate; Crblm, cerebellum; Chroid Ple, choroid plexus; Con, contralateral; CSF, cerebrospinal fluid; D, dorsal; DRG_Cer, dorsal root ganglion, cervical; DRG_Tho, dorsal root ganglion, thoracic; DRG_Lum, dorsal root ganglion, lumbar; EcG, ectolateral gyrus; EnG, entolateral gyrus; FrC, frontal cortex; GFP, green fluorescent protein; Hpc, hippocampus; ICV, intracerebroventricular; Ips, ipsilateral; M, male, MC, motor cortex; mo, month; Olfactory B, olfactory bulb; Optic Chi, optic chiasm; PC, piriform cortex; Periaq G, periaqueductal gray; SC_Cer, spinal cord, cervical; SC_Tho, spinal cord, thoracic; SC_Lum, spinal cord, lumbar; SSC, somatosensory cortex; SSG, suprasylvian gyrus; Tha_1, thalamus ventral anterior nucleus/ventral intermediate (Va/Vl) nucleus; Tha_2, thalamus ventral posterior nucleus (right); Tha_3, thalamus ventral posterior nucleus (left); V, ventral.

Please cite this article in press as: Alam et al., AAV-delivered PPT1 provides long-term neurological benefits in CLN1 mice and achieves therapeutic levels in sheep brain, Molecular Therapy (2025), https://doi.org/10.1016/j.ymthe.2025.07.011

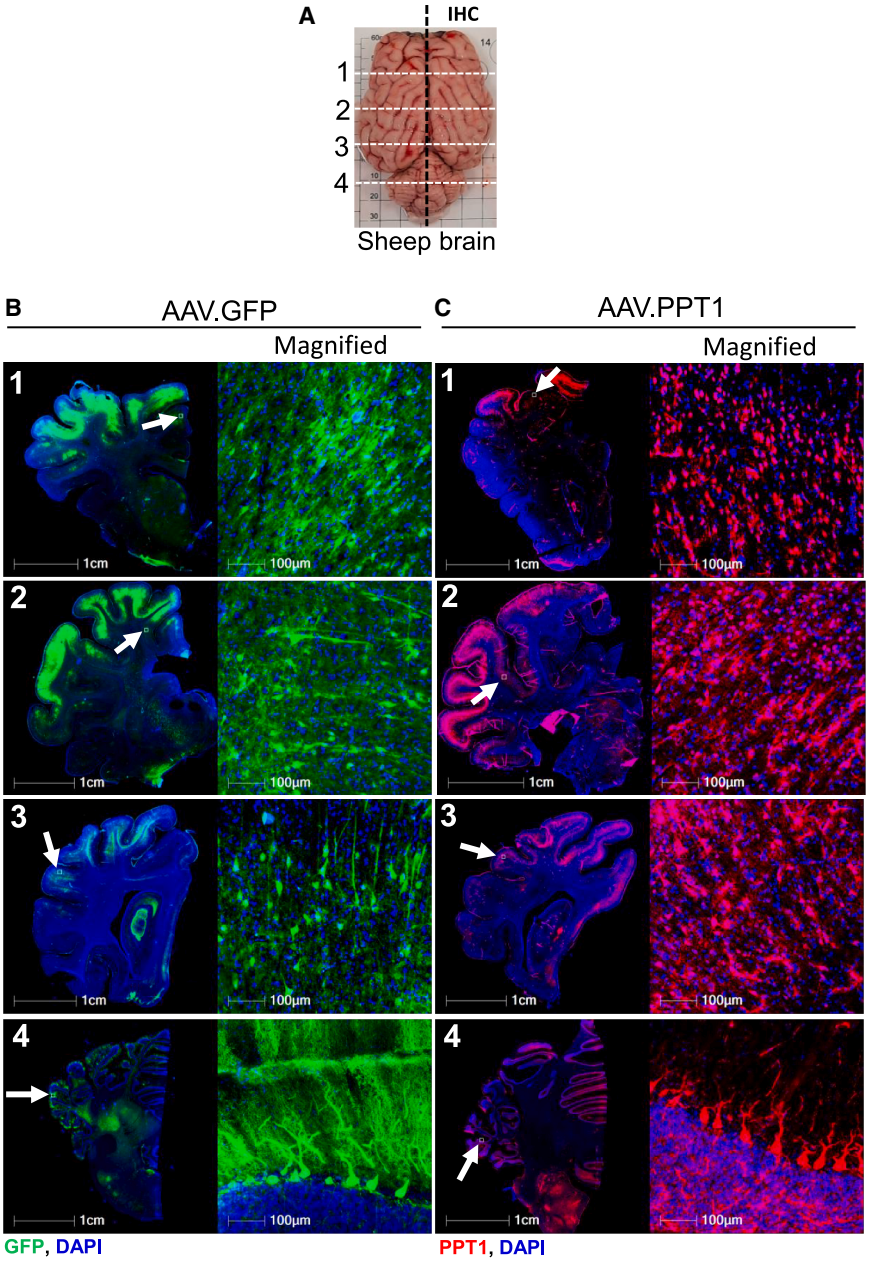

Figure 8. Immunofluorescence detection of PPT1 and GFP in sheep brain

(A) The schematic illustrates the sampling of coronal sections at four distinct planes, labeled 1–4 (denoted by white dotted lines), from the sheep brain hemisphere for immunofluorescence microscopy. Micrographs show (B) GFP (green) and (C) PPT1 (red) expression in brain sections of sheep administered with AAV.GFP or AAV.PPT1 (lead 1), respectively. Areas indicated by white arrows are magnified in adjacent images on the right. Images are representative of two sheep dosed with AAV.GFP and four with AAV.PPT1 vectors. Nuclei (blue) were stained with DAPI. Scale bars as indicated.

The i.c.v. administration of vectors was well tolerated in sheep. None of the animals experienced anaphylactic shock or exhibited any serious adverse effects. Comprehensive assessments of breathing and heart rate, body temperature, body weight, and overall condition scores indicated a favorable safety profile (Figure S12). Neurological evaluations conducted at baseline, 4 weeks, and 8 weeks post dosing included assessment of overall behavior, gait and movement, reflex, proprioception, balance, and vision. At 4 weeks post dosing, transient abnormalities were observed in two animals: one exhibited minor vision irregularities, and another showed brief knuckling behavior in one limb (Figure S13). These findings were deemed clinically insignificant and had resolved by the next assessment (Figure S13).

DISCUSSION

The success of AAV-based therapies for CNS diseases relies on several key factors, including the choice of promoter, AAV capsid, delivery route, and relevant small and large preclinical models. In this study, we carefully considered these factors to ensure the efficacy, durability, safety, and clinical translatability of PPT1 gene therapy for CLN1 disease. Based on the widespread expression of PPT1 in neurons and glia[44] and cellular studies showing impaired glial function in PPT1-deficient cells,[45] we opted for the promoter of the ubiquitously expressed human EF1α gene to enable broad expression. As with many Batten diseases, CLN1 is characterized by widespread neuropathology, emphasizing the necessity of an AAV capsid and delivery route capable of achieving comprehensive CNS distribution. We utilized a capsid with a favorable clinical safety profile[23] and effective CNS tropism demonstrated across multiple species. Intra-CSF routes of administration, which include intrathecal (IT), intra-cisterna magna (ICM), and i.c.v. are under investigation for achieving widespread CNS distribution of AAV-based therapeutics.[42,46] Among all, i.c.v. delivery is highly effective, particularly in neonatal models, making it the preferred approach to maximize CNS exposure during early developmental stages. Guided by biodistribution data in WT neonatal mice, we chose i.c.v. delivery for efficacy testing in a well-characterized CLN1 mouse model.[25] In this model, while significant motor dysfunction typically emerges at 6–7 months of age, recent findings have identified spinal neuropathology as early as 1 month of age.[47] We hypothesized that intervention at P1–P3 would not only enhance biodistribution but also maximize therapeutic benefits by addressing abnormalities at an early stage before their progression.

In this study, we also report a decrease in forelimb grip strength in CLN1 mice, coinciding with severe motor function impairments at 7 months of age. While the cause of diminished grip strength remains unclear, we hypothesize it may stem from impairments in spinal neurons, peripheral nerve damage, intrinsic muscle dysfunction, or their combination. As seen in many neurodegenerative diseases, neuroinflammation in CLN1 is also characterized by increased activation of microglia and astrocytes. Qualitative assessment showed that the overall abundance of glial fibrillary acidic protein (GFAP)-labeled astrocytes in gene therapy-treated CLN1 mice was comparable to WT animals in brain as well as spinal cord. Since PPT1 also works through cell non-autonomous cross-correction mechanisms, we anticipate microglial correction even with limited AAV transduction.

We did not observe candidate- or dose-dependent differences in phenotypic efficacy endpoints. Similarly, the histopathological outcomes presented in Figures 3 and 4 did not indicate any superiority of lead 1 over the unmodified PPT1. Given the widespread supraphysiological levels of PPT1 activity across the CNS (Figures 5 and 6), we were unable to determine a half-maximal effective concentration (EC50) or minimally effective dose in the current dose-ranging study. Given its superior PPT1 secretion and uptake *in vitro* (Figures 1D–1F), higher serum PPT1 activity (Figure S3), and the elevated PPT1 levels in the combined CNS regions in *Ppt1*$^{-/-}$ mice (Figure S9), we anticipate that lead 1 may achieve a lower minimally effective dose compared with unmodified PPT1. Further exploration of lower doses or testing at early symptomatic ages (e.g., 4–6 weeks) may help delineate whether lead 1 outperforms native PPT1.

Durability assessment in *Ppt1*$^{-/-}$ mice at 15 months demonstrated sustained PPT1 expression throughout the CNS, indicating prolonged regulatory element activity. In this study, we also demonstrate the sustained activity of the human EF1α promoter up to 15 months in a disease mouse model. Given the sustained transgene expression, we expect that the treated mice will likely reach their normal lifespan while maintaining strong neurobehavioral function. Long-term studies in large animal or NHP models will provide key insights into the therapeutic durability for clinical use. If these studies mirror the sustained PPT1 expression seen in mice, they will support the feasibility of a one-time gene therapy for CLN1 disease.

For effective clinical translation, it is recommended to test therapeutic agents and delivery methods in both small rodents and large non-rodent gyrencephalic species. Recognizing the benefits of larger brain and neuroanatomical similarities to the human brain,[35,48] we opted to perform biodistribution and tolerability assessment in sheep. The data presented in Figures 7 and 8 demonstrated that the i.c.v. administration of gene therapy vectors in sheep resulted in effective delivery to broad cortical regions, which are highly affected in CLN1 as well as significant delivery to subcortical structures including the thalamus, which shows notable pathology in CLN1 sheep.[10] The thalamus is among the first affected brain regions in the CLN1 mouse model and recognized as a critical target for improving therapeutic outcomes in CLN1 patients.[14,18] However, targeting this region has proven challenging even after combining intrathecal administration with intracranial delivery of AAVs in *Ppt1*$^{-/-}$ mice.[14] In this study, i.c.v. administration effectively targeted the thalamus of *Ppt1*$^{-/-}$ mice, resulting in up to 13-fold increase in mean PPT1 activity compared with WT animals and concomitant protection from storage buildup and astrocytosis. Significant thalamic pathology is seen in mouse models of many LSDs, including NCL diseases.[49–51] Therefore, targeting thalamic pathology through i.c.v. delivery could potentially benefit other LSDs as well.

In a previous study, IT delivery of PPT1 gene therapy in the CLN1 mouse model provided a strong response in the spinal cord but had limited benefit on correcting pathology in the subcortical structures of brain.[14] Its effect on lifespan was also limited, with a median survival of 10 months, whereas in our study, treated mice survived 15 months and are expected to live longer. Additionally, we observed sustained motor function benefits up to 15 months, whereas CLN1 mice treated via IT administration in the previous study began declining in rotarod performance by 7 months, reaching levels similar to untreated animals by 11 months.[14] While the differences in outcomes were likely driven mainly by the delivery route, other factors such as the lower vector dose, a different capsid, and the lack of PPT1 modification also should be considered, as they may have contributed to the therapeutic effects, either individually or in combination. Although IT combined with multipoint intracranial delivery enhanced therapeutic benefits,[14] clinical translation of this approach would be highly challenging. In contrast, i.c.v. administration is well established, safe, and suitable for the delivery of therapeutics in both pediatric and adult populations.[52]

Although neonatal i.c.v. injection in mice may not directly translate to humans due to developmental differences, the results in adult *Ppt1*$^{+/-}$ sheep showing widespread vector transduction and PPT1 expression including deep brain structures of fully mature brains support the potential of this approach for broad CNS correction when dosed in juvenile or adult stages. Efficacy studies in symptomatic CLN1 animals may provide additional insights for informing and refining future clinical trial designs. The lowest effective dose in neonatal *Ppt1*$^{-/-}$ mice (approximating 1×10^{12} vg/g of brain weight) and in adult sheep during the biodistribution study (approximating 1.2×10^{12} vg/g of brain weight) corresponds to approximately 0.4×10^{14} total vg for a newborn and $\sim 1.4 \times 10^{14}$ vg for a 3-year-old CLN1 patient. In mice, this dose resulted in a >3-fold increase in PPT1 activity across most brain regions, while in sheep, activity was elevated by an average of 3.9-fold. Based on this, we anticipate the human dose would likely remain below 1×10^{15} vg, an AAV dose that is approved for trials and shows promising tolerance in 4- to 7-year-olds with Rett syndrome receiving intrathecal gene therapy in an ongoing phase 1/2 trial.[53] Additionally, a preclinical study in rodents and NHPs evaluating AAV9-AP4M1 for hereditary spastic paraplegia type 50 found an acceptable safety profile at

Please cite this article in press as: Alam et al., AAV-delivered PPT1 provides long-term neurological benefits in CLN1 mice and achieves therapeutic levels in sheep brain, Molecular Therapy (2025), https://doi.org/10.1016/j.ymthe.2025.07.011

intrathecal doses up to a human equivalent of 1×10^{15} vg.[54] Nevertheless, the final clinical dose must be carefully determined through dose-ranging and toxicity studies in a relevant preclinical model. While PPT1 gene therapy is expected to be beneficial at all disease stages, its greatest impact is likely at asymptomatic or early symptomatic stages when neuronal networks remain intact, helping preserve function and slow disease progression. Efficacy may be limited in advanced stages due to irreversible neuronal loss.

In conclusion, i.c.v.-delivered AAV-Spark100-PPT1 gene therapy demonstrated robust efficacy and durability in a CLN1 mouse model. With no treatment-related morbidity or mortality in treated CLN1 mice over 15 months and no adverse effects in sheep, these findings highlight a favorable safety profile, marking a critical step toward clinical translation.

MATERIALS AND METHODS

Study design

This study aimed to evaluate a PPT1 variant with increased cross-correction capabilities for broad CNS distribution, long-term efficacy, and durability in the *Ppt1*-deficient mouse model for advancing AAV-based gene therapy for CLN1 disease. Additionally, we conducted a biodistribution assessment in a large animal model to enhance translational relevance. To enhance cross-correction, nine variants of PPT1 were generated and screened by a combination of *in vitro* and *in silico* approaches, leading to the identification of a lead candidate known as lead 1. This candidate was cloned in a single-stranded vector genome and vectorized in a proprietary AAV capsid referred to as Spark100 and subsequently evaluated in animal (mouse and sheep) studies. Unmodified PPT1 (referred to as "native") served as the comparator. *In vivo* efficacy and durability were assessed in $Ppt1^{-/-}$ mice, which closely mimic the human disease.[14,25] Neonatal $Ppt1^{-/-}$ mice (aged P1–P3) received a single i.c.v. injection of either lead 1 or native and were assessed for 15 months. WT and untreated or diluent-treated $Ppt1^{-/-}$ mice were used as controls. Mice (N = 16–20/group, Table S3) were proportionally balanced for gender and randomly assigned to treatment groups. The efficacy readouts included assessments of survival, neurobehavioral functions, and neuropathological analyses of CNS tissues. For the neurobehavioral assessments, motor function, grip strength, and gait were evaluated every 2–3 months, starting from 5 to 7 months of age until 14 months. Neuropathological examinations, which included assessments for brain atrophy, storage accumulation, and astrocytosis, were conducted on tissue collected at 8–10 months of age, which is an end-stage disease in this model. Drug durability, including vector genome presence and PPT1 expression (assessed by IHC and enzymatic activity), was tested at 10 and 15 months of age. The sample sizes, numbers, and composition of replicates were determined based on prior knowledge of this mouse model.[14,25,29,47] A 2-month non-GLP biodistribution and safety study was conducted in 9- to 10-month-old heterozygous healthy $Ppt1^{+/-}$ sheep.[30] Throughout the study, all behavioral, molecular, biochemical, and histological assays were performed by personnel blinded to the treatment and genotype.

PPT1 vector design

The full-length human PPT1 protein consists of 306 amino acids, including an ~27-amino-acid N-terminal signal sequence. While bioinformatic analysis of the PPT1 signal peptide predicts cleavage occurring between residue 22 (alanine) and residue 23 (leucine), our designs were guided by the reported N terminus of the mature PPT1, starting at aspartate at the 27th position.[55] Aspartate functions as a good candidate amino acid for marking a cleavage site between N-terminal signal peptides and a mature polypeptide, however, a net positive charge in the signal peptide is thought to enhance protein secretion, and aspartate is associated with shorter protein half-life for intracellular proteins (N-end rule). For these reasons, we explored the substitution of the native aspartate with either glycine or valine. Nine engineered PPT1 variants were designed by replacing the native signal sequence with signal sequences derived from highly secretable human proteins as listed in Table S1. SignalP 5.0[56] was used to bioinformatically assess the likelihood of correct signal peptide processing for heterologous PPT1 fusion proteins. To further optimize cleavage potential, modifications to the signal peptides or the start of the mature PPT1 sequence were introduced, as described in Table S1. A catalytically inactive variant (referred as dead) was created by substituting two of three active site residues[57] serine115 and histidine289 with alanine (Ser115Ala and His289Ala). The PPT1 transgene expression was driven by a 1,170-base pair (bp) human EF1α promoter. Downstream of the PPT1 transgene, a 225-bp polyadenylation (polyA) signal was included from the bovine growth hormone gene. A 1-kb inert stuffer DNA was added downstream of the PPT1 expression cassette to mitigate potential vector packaging issues. To monitor vector delivery and normalize PPT1 expression in a transfection-based *in vitro* system, an additional 2,034-bp expression cassette consisting of ubiquitin C promoter, TdTomato reporter, and rabbit beta-globin polyadenylation sequence was integrated to the plasmid backbone outside the ITRs. Plasmid construction and sequencing verification were done by Azenta, project 30-615124526R2.

In vitro screening of PPT1 variants

PPT1 knockout ($PPT1^{-/-}$) cells, generated in a human cell line by Synthego Corporation (California, USA), were used for screening. The knockout was validated in a clonal line through PCR, PPT1 activity assays, and capillary-based western analysis, and these cells were subsequently used for screening PPT1 variants. The cells were cultured in Dulbecco's modified Eagle's medium (DMEM) supplemented with 10% fetal bovine serum (FBS) and 1% penicillin/streptomycin under 5% CO_2 at 37°C. Mycoplasma contamination was ruled out by testing every 4–6 weeks. The cells were transfected with AAV plasmids carrying *PPT1* variants using Lipofectamine 3000 (Invitrogen, USA). Media and cells were collected 48 h post-transfection to evaluate PPT1 activity. The cells were harvested by trypsinization, and 10% of the total cells were analyzed for transfection efficiency based on TdTomato expression via flow cytometry (Cytoflex, Beckman Coulter). A total of 20,000 events were recorded for each sample, and TdTomato-positive cells were identified in the ECD channel. The data were analyzed using CytExpert 1.1. The

remaining cells were lysed in McIlvaine's phosphate/citrate buffer (pH 4.5), and the total protein concentration in the lysate was quantified using a bicinchoninic acid (BCA) assay. PPT1 activity was measured using a fluorogenic substrate as described[58] and elaborated below. The activity was first normalized for transfection efficiency. Subsequently, the percentage of PPT1 activity was expressed relative to the cells transfected with unmodified human PPT1 referred as "native," which was set at 100%. In each experiment, cells in three independent wells were transfected per variant, and the experiment was repeated 3–4 times.

PPT1 uptake assay

PPT1$^{-/-}$ cells in a 96-well plate were separately transfected with two lead plasmids and unmodified *PPT1* as a reference. After 48 h, cells were fixed with 4% paraformaldehyde (PFA), permeabilized with 0.05% saponin in PBS for 20 min, and blocked in PBS with 2% goat serum and 0.01% saponin for 30 min at room temperature (RT). Cells were incubated overnight at 4°C with anti-PPT1 antibodies (1:500, Novus Biologicals, NBP2-45388) in blocking buffer, washed three times with PBS, and treated with Alexa Fluor 488-conjugated secondary antibodies (1:1,000, Thermo Fisher Scientific, A-11001) for 1 h at RT. Nuclei were counterstained with Hoechst and cells were imaged using the Opera Phenix Plus system (HH14001000, PerkinElmer) with a 40× water objective. Transfected cells were identified based on TdTomato fluorescence, while cells expressing PPT1 were detected using the 488 channel. Automated quantitative analysis was performed using Harmony 5.1 software that identified cells using Hoechst staining, quantified transfected cells based on TdTomato expression, and detected PPT1-positive cells based on the immunofluorescence signal. Transfected cells were both TdTomato and PPT1 positive. Cells lacking TdTomato fluorescence but showing a PPT1 signal indicated the uptake of secreted PPT1. For quantitative analysis, the ratio of PPT1-positive cells to TdTomato-positive cells was calculated, with a higher ratio suggesting increased uptake and cross-correction potential. For each condition, 30 fields per well were analyzed, and the mean ratio from each well was plotted. Each experiment included 3–4 independently transfected wells for each variant or native control, and the experiment was repeated three times.

In silico immunogenicity assessment

IEDB (Immune Epitope Database) was used to assess the immunogenicity risk of different PPT1 variants, utilizing NetMHCpan for MHC-I and NetMHCIIpan 4.0 for MHC-II.

Vector production

Recombinant AAVs were produced at the Research Vector Core at Spark Therapeutics Inc. Adherent HEK293 cells were transfected using a calcium-phosphate-based triple plasmid system at a 1:1:1 mass ratio. Each DNA combination contained pHelper, pRepCap, and the plasmid carrying the PPT1 transgene of GFP. Cells were harvested 96 h post-transfection, resuspended, and lysed by sonication. The clarified cell lysates were digested with benzonase and precipitated with polyethylene glycol (PEG), further purified by CsCl density-gradient ultracentrifugation and the recovered vectors were exchanged to PBS180/0.001% pluronic F-68 (Gibco 24040-032) via cassette dialysis (Thermo 66455, 10K MWCO). Vector genomes were quantified using TaqMan qPCR with bovine growth hormone (BGH) polyA-specific primers: forward 5′-CTTGCCTTCCTTGACCCT-3′, reverse 5′-CCCAGAATAGAATGACACCTACT-3′ and probe 56-FAM/TTAGGAAAG/ZEN/GACAGTGGGAGTGGC/3IABkFQ. AAV vectors were characterized by SDS-PAGE/Sypro Ruby stain. Endotoxin levels were less than 1 EU/mL, measured using Endosafe LAL cartridges and the Endosafe NexGen PTS device (Charles River, Charleston, SC, USA). Vectors were stored at −80°C until use.

Mouse studies

The pilot biodistribution study (detailed in Table S2) was conducted in C57BL6/J WT mouse pups. For efficacy study, a *Ppt1*-deficient (*Ppt1*$^{-/-}$) mouse model generated by Gupta et al.[25] was used. Male and female mice heterozygous for *Ppt1* loss-of-function mutation (Jax Stock 006566) were cryo-recovered at the Jackson Laboratory and subsequently expanded at PsychoGenics Inc. (Paramus, NJ, USA). Mouse studies were conducted at PsychoGenics Inc, with the pilot biodistribution study under project SPA010 and the efficacy study under project SPA011. Details of groups, dosing scheme, and animal numbers for the efficacy study in *Ppt1*$^{-/-}$ mice are provided in Table S3. Mice were housed in polycarbonate OptiMICE cages under 12/12 light/dark cycles. The room temperature was maintained between 20°C and 23°C with a relative humidity maintained around 50%. Chow and water were provided *ad libitum* for the duration of the study. Animals were checked for survival twice per day. All testing was performed during the animal's light cycle phase.

i.c.v. delivery in mice

Vectors were formulated in a buffer containing 180 mM NaCl, 10 mM sodium phosphate, and 0.001% Pluronic F68 (pH 7.3). In the pilot biodistribution study, WT mice received 1×10^{10} vg or 1×10^{11} vg at P1 (Table S2). The total dose was split equally between hemispheres for bilateral injections, with a volume of 3 μL per hemisphere. Details of groups, dosing scheme, and animal numbers for the efficacy study in *Ppt1*$^{-/-}$ mice are provided in Table S3. In brief, the low-dose group received 1×10^{11} vg, and the high-dose group received 3.82×10^{11} vg/animal, with doses divided equally for bilateral injections. In the low-dose group, mice at P1 received a total of 6 μL injection volume (3 μL per hemisphere). Due to a lower vector titer, the high dose could not be administered in a single day's tolerated volume. We split the 12-μL total dose volume into two 6-μL i.c.v. injections, one hemisphere on P1 and the other on P3, to allow recovery and minimize stress. For injections, pups were briefly anesthetized by placing them on ice for 5–7 min or until the pedal withdrawal reflex was lost, using a barrier (latex or nitrile glove) to prevent direct contact with the ice. To visualize the cerebral ventricles, the pup was positioned above a non-heating light source (LED or fiber optic). Treatments (AAVs or diluent) were administered using a 10-μL Hamilton syringe (1701 RN Model, Cat# 7654-01) and custom Hamilton 30 ½ needles (point style 4, bevel 12°,

Cat# 7803-07). The needle was held in place for 10–20 s post-injection to prevent backflow. After injection, the pups were warmed on a heating pad until they regained normal activity, gently rubbed with home cage bedding to minimize the risk of maternal cannibalism, and then returned to the nest.

Survival analysis

A log rank test for overall differences in survival between treatment groups was performed in "R" using the "*survdiff*" function in package "*survival*" and the associated chi-squared statistic for the hypothesis test. Post hoc pairwise survival difference comparisons with Benjamini-Hochberg correction procedure were performed with "*pairwise_surfdiff*" from the same package. The Kaplan-Meier curves were generated in GraphPad Prism visually displaying the probability of survival over time by treatment group.

Behavioral assessment of mice

Accelerated rotarod performance was measured at 5, 7, 9, 11, and 14 months, while grip strength and gait were assessed at 7, 9, 11, and 14 months. The untreated *Ppt1*$^{-/-}$ mice or those treated with diluent were evaluated only up to 7 months of age, as they did not survive until their next scheduled assessment at 9 months.

Accelerated rotarod

Each session began with a 5-min training trial on the Rotarod, rotating at 4 rpm (Rotamex, OH). After a 1-h rest, animals underwent three 5-min acceleration tests, with speed uniformly increasing to 40 rpm over 300 s. The interval between tests was 30 min. Average of three tests was used for quantitative analysis.

Grip strength

Animals were assessed for forelimb and hindlimb grip strength using SDI Animal Grip Strength System (San Diego Instruments, San Diego, CA). For forelimb testing, the animal was gently lowered onto the platform, and the experimenter applied consistent backward force until the grip was released. For hindlimb testing, the animal was pulled backward along the platform until its hind paws gripped the mesh on the push-pull gauge, and consistent force was applied until release. Each grip strength test included five consecutive trials, with the average value used for analysis.

Gait analysis

Gait assessments were done using NeuroCube, which is an automated behavioral platform that employs computer vision to detect changes in gait geometry and gait dynamics in rodent models.[28] Mice were acclimated in the experimental room for at least an hour prior to the start of testing. Following acclimation, mice were placed into the NeuroCube, which is a rectangular shaped box measuring 35.5 inches long × 9 inches wide × 6 inches high. Mice were given 5 min to move freely within the apparatus. A camera placed under the box records the paw placement and movement of the animals. Digital videos were analyzed through computer-assisted segmentation algorithms as described in detail elsewhere.[28] Fitted parameters were then used to extract clips of motor behavior that were used to extract information about gait geometry and dynamics. Bioinformatics-driven analyses were used to calculate the "percentage discrimination," reflecting the extent to which the cumulative gait parameters of *Ppt1*$^{-/-}$ mice differed from WT animals, and the "percentage retention," measuring the degree to which gene therapy preserved the impaired gait features.

Mouse tissue collection

Mice were anesthetized with isoflurane and CSF was collected via cisterna magna puncture using pulled capillaries. Whole blood was obtained through cardiac puncture, serum was isolated and stored at −80°C until use. Animals were perfused with 10–20 mL of cold (4°C) PBS to remove blood cells. The brain was weighed and dissected into two hemispheres. The left hemisphere was subdivided into various brain regions, including the cortex, hippocampus, thalamus, brainstem, cerebellum, and striatum, each divided into two parts. These samples were snap-frozen in liquid nitrogen and stored at −80°C until shipment. One part of each region was assessed for PPT1 protein analysis whereas the other part was processed for vector distribution. The specific part allocated for each analysis was consistent across all animals. The right hemisphere was fixed in freshly prepared 4% PFA in PBS for 24 h at RT with gentle agitation, then transferred to sterile PBS and stored at 4°C until embedding. The spinal cord was divided into cervical, thoracic, and lumbar regions, with each region further split into anterior and posterior halves. For keeping consistent orientation, posterior halves were marked on the caudal side with tissue marking dye (Epredia Mark-It Tissue Marking Dyes) and fixed in 4% PFA in PBS for 24 h at RT with gentle agitation. Fixed samples were transferred to sterile PBS and subsequently embedded for histological examination. The anterior halves were transversely divided into two pieces, with one piece used for PPT1 protein analysis and the other for vector genome analysis.

Histological analysis of mouse tissue

Tissue embedding, sectioning, staining, and imaging were performed by NeuroScience Associates, Inc. (Knoxville, TN, USA). Brain hemispheres from 40 mice (N = 4–6 animals/group, at age 8–10 months) were embedded in a single gelatin matrix block, and 35-μm-thick coronal sections were cut through the entire depth (rostral to caudal end) of the brain. Similarly, spinal cord segments from 40 mice were embedded in three separate blocks, one for each region (cervical, thoracic, and lumbar) and 35-μm-thick transverse sections were cut throughout the length of each segment. Every 12th free-floating section spaced at 420 μm yielding a total 35 brain sections and 14 spinal cord sections were investigated. PPT1 and GFAP were detected by immunostaining whereas accumulation of AFSM was detected by a direct visualization using 488 channel. Following blocking, tissue sections were incubated overnight at RT with rabbit anti-PPT1 antibody (Sigma, HPA021546, 1:1,500) and chicken anti-GFAP antibody (EnCor, CPCA-GFAP, 1:5,000). Secondary antibodies, anti-rabbit conjugated with Cy3 and anti-chicken conjugated with Alexa Fluor 647, were obtained from Jackson ImmunoResearch. Hoechst counterstaining was performed to label

nuclei. The sections were mounted on gelatin-coated glass slides, air-dried, dehydrated in alcohol, cleared in xylene, and cover-slipped. The entire slide was imaged using an Olympus Slideview VS200 slide scanning system at 20× resolution (0.274 μm/pixel) and images were analyzed using Concentriq platform (Proscia). For cortical thickness, three H&E-stained sections, spaced at 840-μm interval from each mouse were imaged using a Zeiss Axioscan Z1 using 20× air objective at 0.22 μm per pixel. Images were digitally annotated and measured in Halo platform (Indica Labs). The cortical thickness was measured in the motor cortex, spanning from the cingulum bundle to the cortical edge, and in the primary somatosensory cortex, extending from the corpus callosum to the cortical edge.

PPT1 activity assay

PPT1 activity assay was conducted as described by Diggelen et al.[58] The assay quantifies the amount of fluorescent reaction product 4-methylumbelliferyl (4-MU) generated by the cleavage of the substrate 4-methylumbelliferyl-6-thiopalmitoyl-β-D-glucopyranoside (MUTG) because of PPT1's thioesterase activity. Samples were diluted in McIlvaine Buffer, pH 4.5 (Cedarlane, 40120278-1), incubated with substrate mix for the reaction to occur and fluorescence was measured using a plate reader (BioTek Synergy H1, Agilent) with excitation at 368 nm and emission at 448 nm. Activity was quantified based on the standard curve prepared using 4-MU (Sigma-Aldrich, M1381). Additional details are provided in the supplementary section.

Automated capillary electrophoresis western analysis

The size and integrity of PPT1 were assessed using JESS, an automated western system based on capillary electrophoresis, according to the manufacturer's protocol (ProteinSimple, Bio-Techne, USA). A total of 0.2 μg *(in vitro* and mouse samples) or 0.5 μg (sheep samples) of protein was analyzed on a 12- to 300-kDa separation module. PPT1 was detected using rabbit anti-PPT1 antibody (Sigma, HPA021546, 1:25), with a rabbit secondary detection module. Antibody specificity was validated using lysates from *PPT1*$^{-/-}$ cells or brain lysates from untreated mice.

Vector biodistribution

The tissue samples were processed using QIASymphony DNA extraction kits on a Qiasymphony following the Tissue_HC_200_V7_DSP program (Qiagen Cat. 937236). The extracted DNA was measured using a Nanodrop Eight (Thermo Fisher). Vector biodistribution in tissue samples was quantified using TaqMan qPCR (Applied Biosystems, Cat. 4484263). Human PPT1 transgene was detected in mice and sheep treated with PPT1 vectors, while GFP transgene was identified in sheep dosed with GFP vectors using specific primers and probes. The qPCR primers and probes (IDT) used were as follows: for PPT1, forward primer 5′-ATG CAG GAC AGC TAG TGT TTC TGGC-3′, reverse primer 5′-TGG CTG CAG GAA TTC AGC TCT AGATC-3′, and probe 5′-/56-FAM/ATG CCC ACA/ZEN/TCA TAC CAT TCC TTG G/3IABkFQ-3′; and for GFP, forward primer 5′-CGT GCC TTC CTT GAC CCT-3′, reverse primer 5′-CCC AGA ATA GAA TGA CAC CTA CT-3′, and probe 5′-/56-FAM/TTA GGA AAG/ZEN/GAC AGT GGG AGT GGC-3′. The qPCR assays were optimized for vector quantification using a standard curve prepared with linearized plasmid standards carrying the respective transgenes, diluted in 20 ng/μL of sheep (Zyagen, SG-201) or mouse genomic DNA (Zyagen, MG-314). These assays were validated to ensure no cross-reactivity was observed with animal genomic DNA and demonstrated a sensitivity of 10 copies per PCR reaction in 200 ng of genomic DNA, corresponding to a detection limit of 50 copies/μg of genomic DNA. Vector genome copy numbers per diploid genome (VGCN/d.g.) were calculated using the genomic DNA weight of a single cell per diploid genome, based on reference genome information from NCBI: mouse genome size (NCBI RefSeq assembly GCF_000001635.27) and sheep genome size (NCBI RefSeq assembly GCF_016772045.2).

Biodistribution study in sheep

A 2-month-long biodistribution and preliminary safety study was conducted in 9- to 10-month-old *Ppt1*$^{+/-}$ male sheep. The experimental animals were generated by breeding heterozygous sheep[30] at the Roslin Institute, University of Edinburgh, United Kingdom. Four animals received a 2-mL dose of vector containing 1×10^{14} vg of lead 1 (Spark100.PPT1 also referred as AAV.PPT1) via c-arm fluoroscopy guided unilateral i.c.v. delivery, while two control animals were administered the same dose and volume of an AAV expressing GFP (Spark100.GFP, also referred as AAV.GFP). In the GFP vector, all components of vector genome elements were similar to PPT1 vector except the *PPT1* was replaced with GFP transgene. At pre-dosing and 1- and 2-months post dosing, animals were assessed by a battery of behavioral assessments and clinical functional tests (Figure S13) as described previously.[30,59]

Neurosurgery and vector administration in sheep

All surgical procedures were performed by a veterinary surgical specialist with guidance from a human clinical radiologist. Sheep were anesthetized as described below and placed in sternal recumbency with the head secured in a brace. Head positioning was checked with an initial preoperative X-ray to ensure a true lateral view was obtained. The skin overlying the frontal bone was clipped and aseptically prepared for surgery. The injection site for craniostomy was selected based on several factors: the interaural (IAP) and orbitomeatal (OMP) planes were used to prevent a posterior approach that could affect the visual cortex, while the anterior limit was determined by frontal sinus development and the need to avoid the somatosensory cortex. The surgical site was draped, and surgical landmarks were identified. Surgical planning for the craniotomy site and needle placement into the ventricle was then performed. Using a sterile marker pen, a line was drawn down the midline of the frontal bone and a second line was drawn joining the caudal limits of the left and right orbits. A needle was placed on the midline of the skull in the coronal suture. The craniotomy site was identified approximately 35 mm cranial to the coronal suture needle and 10 mm lateral to the midline. This spot is approximately 20 mm caudal to the caudal limits of the orbits. A temporary marker needle was placed through the skin and anchored in the underlying bone. An intra-operative

X-ray was used to confirm correct needle positioning. A full-thickness skin incision was made parallel to and including the craniotomy site needle. Self-retaining retractors and a periosteal elevator were used expose the underlying cranium and identify the craniotomy site. The needle was removed and a 2-mm drill bit, attached to a hand drill, was used to create the craniotomy. Using a blunt-ended instrument, the dura was penetrated and an 18-G blunt-ended needle was advanced through the brain parenchyma toward the lateral ventricle. Intra-operative X-rays were used to assess needle position, angulation, and depth. To assess the needle position within the ventricle, an injection of 0.1–0.3 mL contrast (50% Omnipaque 350 mg/mL, GE Healthcare) was made, and an intra-operative X-ray was taken to ensure contrast was visible within the ventricle. If required, the needle was repositioned until confirmed within the ventricle. The AAV vector was injected at a rate of 100 μL per 30 s. Following completion of the injection, a final contrast injection was performed to ensure AAV delivery was completed entirely within the ventricle. The needle was removed, and the subcutaneous tissues and skin were closed routinely. The sheep was then recovered from anesthesia.

Pre- and post-operative anesthesia and care of sheep

Sheep were sedated with medetomidine (5 μg/kg, "Medetor"; Virbac, Suffolk, UK), ketamine (0.5 mg/kg, "Ketamidor"; Chanelle Vet, Berkshire, UK), combined and administered by slow intravenous injection, via a 16-G cannula placed into the jugular vein. When profound sedation was present (1–3 min), anesthesia was induced with propofol ("Propofol 1% w/v"; Fresenius Kabi, Cheshire, UK) administered to effect (2–3 mg/kg) by slow intravenous injection. Once the sheep was unconscious, its trachea was intubated with an endotracheal tube (8.0–9.0 mm internal diameter) and the cuff inflated. The sheep remained in sternal recumbency throughout anesthesia, which was maintained using isoflurane ("IsoFlo"; Zoetis, Surrey, UK) vaporized in oxygen and medical air (1:1), administered via a "circle" rebreathing system. Mechanical ventilation was imposed using a Datex Aestiva 5 anesthesia workstation (Datex Ohmeda, Helsinki, Finland) in volume control mode, with a tidal volume of 8–10 mL kg^{-1} and positive end expiratory pressure of 2–4 cmH_2O. Respiratory rate and/or tidal volume were adjusted to avoid excessive hypercapnia ($Fe'CO_2$ 4.7–7.3 kPa). Physiological monitoring during anesthesia consisted of electrocardiogram; pulse oximetry; inspired and expired concentrations of O_2, CO_2, and inhalant agent; spirometry; and temperature (intranasal or rectal) ("S/5 Compact"; Datex Ohmeda, Helsinki, Finland). Blood pressure was monitored invasively, using an arterial cannula (20G or 22G) placed in the central auricular artery, or noninvasively, using an appropriately sized cuff placed around a distal limb. Intravenous fluid therapy was Hartmann's solution ("Vetivex No11"; Dechra, Shrewsbury) infused at 4–6 mL kg hr^{-2}. For surgical procedures, analgesia was provided using local infiltration of the surgical site with bupivacaine ("Bupivacaine hydrochloride 0.5%"; Aspen Pharma, Dublin, Ireland) and lidocaine ("Lidocaine hydrochloride 2%"; Hameln, Gloucester, UK) mixed in a 1:1 ratio. Meloxicam (1.0 mg/kg ("Metacam"; Boehringer Ingelheim Animal Health, Berkshire, UK) was injected subcutaneously. Perioperative antibiosis was provided by intramuscular amoxicillin (15 mg/kg "Betamox LA"; Norbrook Laboratories, Northamptonshire, UK). On completion of the procedure, isoflurane administration was ended, the animals were weaned off the ventilator, and 25 μg/kg atipamezole was administered intramuscularly ("Antisedan"; Vetoquinol, Buckinghamshire, UK) to hasten recovery. The trachea was extubated once spontaneous breathing and active chewing and/or swallowing were present. The endotracheal tube was withdrawn with the cuff partially inflated to remove any accumulated oropharyngeo-tracheal fluid. After this, the intravenous cannula was removed. The sheep were monitored continuously until standing.

Collection of tissues from sheep

At 2 months post dosing, sheep were euthanized using overdose of pentobarbital. Death was confirmed by cessation of circulation (by auscultation of the heart). The brains were extracted and placed in cold saline for 20 min, with a fresh saline change after the first 10 min. Using a custom-made brain matrix, 7-mm-thick coronal slabs were cut yielding 10 slabs per brain. A medial cut separated the left and right hemispheres. For collecting samples for molecular and biochemical analysis, brain regions were identified using the sheep brain atlas.[60,61] Three-millimeter tissue punches were collected using a biopsy punch or manual microdissection, from the ipsilateral slabs (the injection side). A few punches were also collected from the selected brain regions of the contralateral slabs for comparative analysis. Punches were collected in pairs from adjacent regions: one for vector DNA and the other for protein analysis. These samples were snap-frozen in liquid nitrogen and stored at −80°C. Slabs from the contralateral hemisphere were drop fixed in 10% formalin for 96 h at 4°C, with a fixative exchange after 48 h. After fixation, samples were transferred to sterile PBS and processed for cryosectioning. Peripheral tissues, blood, CSF, spinal cord, and DRGs from cervical, thoracic, and lumbar regions were also collected and appropriately stored.

Immunofluorescence analysis of sheep tissue

Immunostaining of sheep brain was performed on 30-μm free-floating sections of fixed-frozen sheep brains. Tissue washes and reagent dilutions were done in 1X PBS. Sections were blocked with 5% BSA in 0.3% Triton X-100 for 1 h, then incubated overnight at 4°C with anti-PPT1 antibodies (Sigma-Aldrich, HPA021546, 1:500). Cy3-conjugated anti-rabbit secondary antibodies (Jackson ImmunoResearch, 711-165-152, 1:1,000) were applied at room temperature for 2 h. GFP was detected directly in the 488 channel without the need for immunostaining. Nuclei were stained with DAPI (Fisher #62248, 1:1,000). Slides were mounted with Fluoromount (Sigma-Aldrich, f4680-25 mL) and scanned on a Zeiss Axioscan Z1 at 10× with 0.46 μm per pixel.

Study approval

Experimentation on mice were carried out as per Institutional Animal Care and Use Committee (IACUC) (#IACUC 271_0315 V4) policies of PsychoGenics Inc. Mice were humanely euthanized at

defined time points or when found morbid (severe lethargy, lack of movement, hunched posture, difficulty in breathing, skin tenting) as accordance with IACUC. Sheep studies were reviewed and approved by the Animal Welfare and Ethical Review Board (AWERB) of the Roslin Institute and conducted under the authority of the UK Home Office (equivalent of an IACUC). The work in sheep was carried out under license number PB2318334.

Statistical analysis

All quantitative data in the figures, unless otherwise specified, are presented as mean ± SD and analyzed using GraphPad Prism software (version 10.3.0) or MS Excel. Comparisons between the two groups were done using unpaired two-tailed Student's t test. Differences between more than two groups were carried out using 1-way ANOVA with Tukey's or Dunnett's correction for relevant pairwise comparisons. Weighted two-way ANOVA was done for testing the cumulative difference in PPT1 activity between the control and test group in sheep brain. Difference in survival was tested by log rank test in R using the '*survdiff*' function and the associated chi-squared statistic for the hypothesis test. Benjamini-Hochberg correction was performed for post hoc pairwise survival difference comparisons. For all statistical analysis, $p < 0.05$ was considered significant. The statistical analysis performed for each dataset is indicated in the figure legends.

DATA AVAILABILITY

All data are provided in the main text or supplementary section, with no data deposited in external repositories. All associated data presented here are available on reasonable request from the corresponding authors (M.S.A. and M.G.B.).

ACKNOWLEDGMENTS

We thank Xin Zhang, Lihua Shi, and Charmaine Azutillo for vector support; Bo Wang for histology assistance; Manjunatha Benakanakere for *in silico* immunogenicity assessment; and Eric Kostuk, Aidan Smith, and Karthik Ramanathan for their contribution in initial mouse studies. We would like to thank all members of the ALLMoND (Academic Led Livestock Models of Neurological Disorders) research group and all members of the LARIF (Large Animal Research & Imaging Facility, University of Edinburgh) team. This work was supported by Spark Therapeutics, Inc. We are thankful for BBSRC funding underpinning S.L.E. and T.M.W. via Institute Strategic Program Grant funding (reference BB/X010945/1).

AUTHOR CONTRIBUTIONS

M.S.A., M.G.B., and E.R. conceptualized the project, designed the studies and experiments, and supervised the research. M.S.A. and D.M.C. designed the constructs. A.K. and M.S.A. conducted *in vitro* experiments and analyzed data. M.S.A., A.K., J.W., M. D., D.P., G.R.-P., M.N., R.G., C.L., M.B., and H.B. developed the methodologies and conducted the investigation of animal samples. M.S.A., A.K., D.M.C., M.G.B., and E.R. visualized and analyzed the cellular and mouse data. M.S.A. and G.A. performed statistical analysis. S.L.E., T.M.W., M.S.A., J.M., M.G.B., E.R., M.G., G.T., E.C., F.M., J.N., S.N.G., S. G.L., and R.G. designed the study in sheep, conducted in-life experimentation, collected samples, and analyzed the data. M.S.A., J.M., A.K., M.G.B., E.R., D.M.C., M.B., C.L., R. G., S.L.E., and T.M.W. contributed to writing and editing. M.S.A. and E.R. wrote the original draft. All authors reviewed and edited the manuscript.

DECLARATION OF INTERESTS

M.S.A., A.K., D.M.C., J.M., M.G.B., and E.R. are co-inventors on the following patent entitled "PPT1 Gene Therapy," Provisional Application No. 63/491205. M.S.A., A.K., D.M.C., J.W., M.D., D.P., G.R.-P., M.N., M.B., H.B., C.L., R.G., G.A., J.M., M.G.B., and E.R. are either present or past paid employees of Spark Therapeutics, Inc., a Roche company, and may hold equity in the organization.

SUPPLEMENTAL INFORMATION

Supplemental information can be found online at https://doi.org/10.1016/j.ymthe.2025.07.011.

REFERENCES

1. Simonati, A., and Williams, R.E. (2022). Neuronal Ceroid Lipofuscinosis: The Multifaceted Approach to the Clinical Issues, an Overview. Front. Neurol. *13*, 811686. https://doi.org/10.3389/fneur.2022.811686.

2. Schulz, A., Kohlschütter, A., Mink, J., Simonati, A., and Williams, R. (2013). NCL diseases - clinical perspectives. Biochim. Biophys. Acta *1832*, 1801–1806. https://doi.org/10.1016/j.bbadis.2013.04.008.

3. Vesa, J., Hellsten, E., Verkruyse, L.A., Camp, L.A., Rapola, J., Santavuori, P., Hofmann, S.L., and Peltonen, L. (1995). Mutations in the palmitoyl protein thioesterase gene causing infantile neuronal ceroid lipofuscinosis. Nature *376*, 584–587. https://doi.org/10.1038/376584a0.

4. Augustine, E.F., Adams, H.R., de Los Reyes, E., Drago, K., Frazier, M., Guelbert, N., Laine, M., Levin, T., Mink, J.W., Nickel, M., et al. (2021). Management of CLN1 Disease: International Clinical Consensus. Pediatr. Neurol. *120*, 38–51. https://doi.org/10.1016/j.pediatrneurol.2021.04.002.

5. Santavuori, P., Haltia, M., Rapola, J., and Raitta, C. (1973). Infantile type of so-called neuronal ceroid-lipofuscinosis. 1. A clinical study of 15 patients. J. Neurol. Sci. *18*, 257–267. https://doi.org/10.1016/0022-510x(73)90075-0.

6. Puhl, A.C., and Ekins, S. (2022). Advancing the Research and Development of Enzyme Replacement Therapies for Lysosomal Storage Diseases. GEN. Biotechnol. *1*, 156–162. https://doi.org/10.1089/genbio.2021.0013.

7. Platt, F.M. (2018). Emptying the stores: lysosomal diseases and therapeutic strategies. Nat. Rev. Drug Discov. *17*, 133–150. https://doi.org/10.1038/nrd.2017.214.

8. Schulz, A., Specchio, N., de Los Reyes, E., Gissen, P., Nickel, M., Trivisano, M., Aylward, S.C., Chakrapani, A., Schwering, C., Wibbeler, E., et al. (2024). Safety and efficacy of cerliponase alfa in children with neuronal ceroid lipofuscinosis type 2 (CLN2 disease): an open-label extension study. Lancet Neurol. *23*, 60–70. https://doi.org/10.1016/S1474-4422(23)00384-8.

9. Schulz, A., Ajayi, T., Specchio, N., de Los Reyes, E., Gissen, P., Ballon, D., Dyke, J.P., Cahan, H., Slasor, P., Jacoby, D., et al. (2018). Study of Intraventricular Cerliponase Alfa for CLN2 Disease. N. Engl. J. Med. *378*, 1898–1907. https://doi.org/10.1056/NEJMoa1712649.

10. Nelvagal, H.R., Eaton, S.L., Wang, S.H., Eultgen, E.M., Takahashi, K., Le, S.Q., Nesbitt, R., Dearborn, J.T., Siano, N., Puhl, A.C., et al. (2022). Cross-species efficacy of enzyme replacement therapy for CLN1 disease in mice and sheep. J. Clin. Invest. *132*, e163107. https://doi.org/10.1172/JCI163107.

11. Hahn, A., Sato, Y., Ikeda, T., Sonoda, H., Schmidt, M., Pfrimmer, C., Boado, R.J., and Pardridge, W.M. (2022). Treatment of CLN1 disease with a blood-brain barrier penetrating lysosomal enzyme. Mol. Genet. Metab. Rep. *33*, 100930. https://doi.org/10.1016/j.ymgmr.2022.100930.

12. Ziolkowska, E.A., Jansen, M.J., Williams, L.L., Wang, S.H., Eultgen, E.M., Takahashi, K., Le, S.Q., Nelvagal, H.R., Sharma, J., Sardiello, M., et al. (2025). Gene therapy ameliorates bowel dysmotility and enteric neuron degeneration and extends survival in lysosomal storage disorder mouse models. Sci. Transl Med. *17*, eadj1445. https://doi.org/10.1126/scitranslmed.adj1445.

13. Griffey, M., Bible, E., Vogler, C., Levy, B., Gupta, P., Cooper, J., and Sands, M.S. (2004). Adeno-associated virus 2-mediated gene therapy decreases autofluorescent storage material and increases brain mass in a murine model of infantile neuronal ceroid lipofuscinosis. Neurobiol. Dis. *16*, 360–369. https://doi.org/10.1016/j.nbd.2004.03.005.

14. Shyng, C., Nelvagal, H.R., Dearborn, J.T., Tyynelä, J., Schmidt, R.E., Sands, M.S., and Cooper, J.D. (2017). Synergistic effects of treating the spinal cord and brain in CLN1 disease. Proc. Natl. Acad. Sci. USA *114*, E5920–E5929. https://doi.org/10.1073/pnas.1701832114.

15. Liu, W., Kleine-Holthaus, S.M., Herranz-Martin, S., Aristorena, M., Mole, S.E., Smith, A.J., Ali, R.R., and Rahim, A.A. (2020). Experimental gene therapies for the NCLs. Biochim. Biophys. Acta Mol. Basis Dis. *1866*, 165772. https://doi.org/10.1016/j.bbadis.2020.165772.

16. Kotnik, P. (2024). Joint Statement to the Global Batten Disease Community. https://bdsrafoundation.org/joint-statement-to-the-global-batten-disease-community-taysha/.
17. Galvin, N., Vogler, C., Levy, B., Kovacs, A., Griffey, M., and Sands, M.S. (2008). A murine model of infantile neuronal ceroid lipofuscinosis-ultrastructural evaluation of storage in the central nervous system and viscera. Pediatr. Dev. Pathol. *11*, 185–192. https://doi.org/10.2350/07-03-0242.1.
18. Kielar, C., Maddox, L., Bible, E., Pontikis, C.C., Macauley, S.L., Griffey, M.A., Wong, M., Sands, M.S., and Cooper, J.D. (2007). Successive neuron loss in the thalamus and cortex in a mouse model of infantile neuronal ceroid lipofuscinosis. Neurobiol. Dis. *25*, 150–162. https://doi.org/10.1016/j.nbd.2006.09.001.
19. Macauley, S.L., Wozniak, D.F., Kielar, C., Tan, Y., Cooper, J.D., and Sands, M.S. (2009). Cerebellar pathology and motor deficits in the palmitoyl protein thioesterase 1-deficient mouse. Exp. Neurol. *217*, 124–135. https://doi.org/10.1016/j.expneurol.2009.01.022.
20. Sands, M.S., and Davidson, B.L. (2006). Gene therapy for lysosomal storage diseases. Mol. Ther. *13*, 839–849. https://doi.org/10.1016/j.ymthe.2006.01.006.
21. Costa-Verdera, H., Collaud, F., Riling, C.R., Sellier, P., Nordin, J.M.L., Preston, G.M., Cagin, U., Fabregue, J., Barral, S., Moya-Nilges, M., et al. (2021). Hepatic expression of GAA results in enhanced enzyme bioavailability in mice and non-human primates. Nat. Commun. *12*, 6393. https://doi.org/10.1038/s41467-021-26744-4.
22. Puzzo, F., Colella, P., Biferi, M.G., Bali, D., Paulk, N.K., Vidal, P., Collaud, F., Simon-Sola, M., Charles, S., Hardet, R., et al. (2017). Rescue of Pompe disease in mice by AAV-mediated liver delivery of secretable acid alpha-glucosidase. Sci. Transl. Med. *9*, eaam6375. https://doi.org/10.1126/scitranslmed.aam6375.
23. George, L.A., Sullivan, S.K., Giermasz, A., Rasko, J.E.J., Samelson-Jones, B.J., Ducore, J., Cuker, A., Sullivan, L.M., Majumdar, S., Teitel, J., et al. (2017). Hemophilia B Gene Therapy with a High-Specific-Activity Factor IX Variant. N. Engl. J. Med. *377*, 2215–2227. https://doi.org/10.1056/NEJMoa1708538.
24. NCT06826612. A Randomized Study of SPK-10001 Gene Therapy in Participants With Huntington's Disease. https://clinicaltrials.gov/study/NCT06826612.
25. Gupta, P., Soyombo, A.A., Atashband, A., Wisniewski, K.E., Shelton, J.M., Richardson, J.A., Hammer, R.E., and Hofmann, S.L. (2001). Disruption of PPT1 or PPT2 causes neuronal ceroid lipofuscinosis in knockout mice. Proc. Natl. Acad. Sci. USA *98*, 13566–13571. https://doi.org/10.1073/pnas.251485198.
26. Roberts, M.S., Macauley, S.L., Wong, A.M., Yilmas, D., Hohm, S., Cooper, J.D., and Sands, M.S. (2012). Combination small molecule PPT1 mimetic and CNS-directed gene therapy as a treatment for infantile neuronal ceroid lipofuscinosis. J. Inherit. Metab. Dis. *35*, 847–857. https://doi.org/10.1007/s10545-011-9446-x.
27. Sun, A. (2018). Lysosomal storage disease overview. Ann. Transl. Med. *6*, 476. https://doi.org/10.21037/atm.2018.11.39.
28. Dave, K.D., De Silva, S., Sheth, N.P., Ramboz, S., Beck, M.J., Quang, C., Switzer, R.C., 3rd, Ahmad, S.O., Sunkin, S.M., Walker, D., et al. (2014). Phenotypic characterization of recessive gene knockout rat models of Parkinson's disease. Neurobiol. Dis. *70*, 190–203. https://doi.org/10.1016/j.nbd.2014.06.009.
29. Sarkar, C., Chandra, G., Peng, S., Zhang, Z., Liu, A., and Mukherjee, A.B. (2013). Neuroprotection and lifespan extension in Ppt1(-/-) mice by NtBuHA: therapeutic implications for INCL. Nat. Neurosci. *16*, 1608–1617. https://doi.org/10.1038/nn.3526.
30. Eaton, S.L., Proudfoot, C., Lillico, S.G., Skehel, P., Kline, R.A., Hamer, K., Rzechorzek, N.M., Clutton, E., Gregson, R., King, T., et al. (2019). CRISPR/Cas9 mediated generation of an ovine model for infantile neuronal ceroid lipofuscinosis (CLN1 disease). Sci. Rep. *9*, 9891. https://doi.org/10.1038/s41598-019-45859-9.
31. Haltia, M. (2003). The neuronal ceroid-lipofuscinoses. J. Neuropathol. Exp. Neurol. *62*, 1–13. https://doi.org/10.1093/jnen/62.1.1.
32. Bible, E., Gupta, P., Hofmann, S.L., and Cooper, J.D. (2004). Regional and cellular neuropathology in the palmitoyl protein thioesterase-1 null mutant mouse model of infantile neuronal ceroid lipofuscinosis. Neurobiol. Dis. *16*, 346–359. https://doi.org/10.1016/j.nbd.2004.02.010.
33. Das, A.K., Becerra, C.H., Yi, W., Lu, J.Y., Siakotos, A.N., Wisniewski, K.E., and Hofmann, S.L. (1998). Molecular genetics of palmitoyl-protein thioesterase deficiency in the U.S. J. Clin. Invest. *102*, 361–370. https://doi.org/10.1172/JCI3112.
34. Miller, J.N., Kovács, A.D., and Pearce, D.A. (2015). The novel Cln1(R151X) mouse model of infantile neuronal ceroid lipofuscinosis (INCL) for testing nonsense suppression therapy. Hum. Mol. Genet. *24*, 185–196. https://doi.org/10.1093/hmg/ddu428.
35. Banstola, A., and Reynolds, J.N.J. (2022). The Sheep as a Large Animal Model for the Investigation and Treatment of Human Disorders. Biology (Basel) *11*, 1251. https://doi.org/10.3390/biology11091251.
36. Murray, S.J., and Mitchell, N.L. (2022). The Translational Benefits of Sheep as Large Animal Models of Human Neurological Disorders. Front. Vet. Sci. *9*, 831838. https://doi.org/10.3389/fvets.2022.831838.
37. Zilles, K., Palomero-Gallagher, N., and Amunts, K. (2013). Development of cortical folding during evolution and ontogeny. Trends Neurosci. *36*, 275–284. https://doi.org/10.1016/j.tins.2013.01.006.
38. Katz, M.L., Coates, J.R., Sibigtroth, C.M., Taylor, J.D., Carpentier, M., Young, W.M., Wininger, F.A., Kennedy, D., Vuillemenot, B.R., and O'Neill, C.A. (2014). Enzyme replacement therapy attenuates disease progression in a canine model of late-infantile neuronal ceroid lipofuscinosis (CLN2 disease). J. Neurosci. Res. *92*, 1591–1598. https://doi.org/10.1002/jnr.23423.
39. Mitchell, N.L., Russell, K.N., Wellby, M.P., Wicky, H.E., Schoderboeck, L., Barrell, G.K., Melzer, T.R., Gray, S.J., Hughes, S.M., and Palmer, D.N. (2018). Longitudinal In Vivo Monitoring of the CNS Demonstrates the Efficacy of Gene Therapy in a Sheep Model of CLN5 Batten Disease. Mol. Ther. *26*, 2366–2378. https://doi.org/10.1016/j.ymthe.2018.07.015.
40. Mitchell, N.L., Murray, S.J., Wellby, M.P., Barrell, G.K., Russell, K.N., Deane, A.R., Wynyard, J.R., Palmer, M.J., Pulickan, A., Prendergast, P.M., et al. (2023). Long-term safety and dose escalation of intracerebroventricular CLN5 gene therapy in sheep supports clinical translation for CLN5 Batten disease. Front. Genet. *14*, 1212228. https://doi.org/10.3389/fgene.2023.1212228.
41. NCT05228145. Gene Therapy Study for Children With CLN5 Batten Disease (CLN5-200). https://clinicaltrials.gov/study/NCT05228145.
42. Chen, X., Lim, D.A., Lawlor, M.W., Dimmock, D., Vite, C.H., Lester, T., Tavakkoli, F., Sadhu, C., Prasad, S., and Gray, S.J. (2023). Biodistribution of Adeno-Associated Virus Gene Therapy Following Cerebrospinal Fluid-Directed Administration. Hum. Gene Ther. *34*, 94–111. https://doi.org/10.1089/hum.2022.163.
43. Hinderer, C., Bell, P., Vite, C.H., Louboutin, J.P., Grant, R., Bote, E., Yu, H., Pukenas, B., Hurst, R., and Wilson, J.M. (2014). Widespread gene transfer in the central nervous system of cynomolgus macaques following delivery of AAV9 into the cisterna magna. Mol. Ther. Methods Clin. Dev. *1*, 14051. https://doi.org/10.1038/mtm.2014.51.
44. Atlas, H.P. (2024). https://www.proteinatlas.org/ENSG00000131238-PPT1/brain.
45. Lange, J., Haslett, L.J., Lloyd-Evans, E., Pocock, J.M., Sands, M.S., Williams, B.P., and Cooper, J.D. (2018). Compromised astrocyte function and survival negatively impact neurons in infantile neuronal ceroid lipofuscinosis. Acta Neuropathol. Commun. *6*, 74. https://doi.org/10.1186/s40478-018-0575-4.
46. Massaro, G., Geard, A.F., Liu, W., Coombe-Tennant, O., Waddington, S.N., Baruteau, J., Gissen, P., and Rahim, A.A. (2021). Gene Therapy for Lysosomal Storage Disorders: Ongoing Studies and Clinical Development. Biomolecules *11*, 611. https://doi.org/10.3390/biom11040611.
47. Nelvagal, H.R., Dearborn, J.T., Ostergaard, J.R., Sands, M.S., and Cooper, J.D. (2021). Spinal manifestations of CLN1 disease start during the early postnatal period. Neuropathol. Appl. Neurobiol. *47*, 251–267. https://doi.org/10.1111/nan.12658.
48. Banstola, A., and Reynolds, J.N.J. (2022). Mapping sheep to human brain: The need for a sheep brain atlas. Front. Vet. Sci. *9*, 961413. https://doi.org/10.3389/fvets.2022.961413.
49. Cooper, J.D., Tarczyluk, M.A., and Nelvagal, H.R. (2015). Towards a new understanding of NCL pathogenesis. Biochim. Biophys. Acta *1852*, 2256–2261. https://doi.org/10.1016/j.bbadis.2015.05.014.
50. Para, C., Bose, P., and Pshezhetsky, A.V. (2020). Neuropathophysiology of Lysosomal Storage Diseases: Synaptic Dysfunction as a Starting Point for Disease Progression. J. Clin. Med. *9*, 616. https://doi.org/10.3390/jcm9030616.

51. Autti, T., Joensuu, R., and Aberg, L. (2007). Decreased T2 signal in the thalami may be a sign of lysosomal storage disease. Neuroradiology *49*, 571–578. https://doi.org/10.1007/s00234-007-0220-6.

52. Cohen-Pfeffer, J.L., Gururangan, S., Lester, T., Lim, D.A., Shaywitz, A.J., Westphal, M., and Slavc, I. (2017). Intracerebroventricular Delivery as a Safe, Long-Term Route of Drug Administration. Pediatr. Neurol. *67*, 23–35. https://doi.org/10.1016/j.pediatrneurol.2016.10.022.

53. Neurogene (2024). Neurogene Reports Positive Interim Efficacy Data from First Four Low-Dose Pediatric Participants in NGN-401 Gene Therapy Clinical Trial for Rett Syndrome. https://ir.neurogene.com/news-releases/news-release-details/neurogene-reports-positive-interim-efficacy-data-first-four-low.

54. Chen, X., Dong, T., Hu, Y., De Pace, R., Mattera, R., Eberhardt, K., Ziegler, M., Pirovolakis, T., Sahin, M., Bonifacino, J.S., et al. (2023). Intrathecal AAV9/AP4M1 gene therapy for hereditary spastic paraplegia 50 shows safety and efficacy in preclinical studies. J. Clin. Invest. *133*, e164575. https://doi.org/10.1172/JCI164575.

55. Vaca Jacome, A.S., Rabilloud, T., Schaeffer-Reiss, C., Rompais, M., Ayoub, D., Lane, L., Bairoch, A., Van Dorsselaer, A., and Carapito, C. (2015). N-terminome analysis of the human mitochondrial proteome. Proteomics *15*, 2519–2524. https://doi.org/10.1002/pmic.201400617.

56. SignalP-5.0. Signal peptide and cleavage sites in gram+, gram- and eukaryotic amino acid sequences. https://services.healthtech.dtu.dk/services/SignalP-5.0/.

57. Bellizzi, J.J., 3rd, Widom, J., Kemp, C., Lu, J.Y., Das, A.K., Hofmann, S.L., and Clardy, J. (2000). The crystal structure of palmitoyl protein thioesterase 1 and the molecular basis of infantile neuronal ceroid lipofuscinosis. Proc. Natl. Acad. Sci. USA *97*, 4573–4578. https://doi.org/10.1073/pnas.080508097.

58. van Diggelen, O.P., Keulemans, J.L., Winchester, B., Hofman, I.L., Vanhanen, S.L., Santavuori, P., and Voznyi, Y.V. (1999). A rapid fluorogenic palmitoyl-protein thioesterase assay: pre- and postnatal diagnosis of INCL. Mol. Genet. Metab. *66*, 240–244. https://doi.org/10.1006/mgme.1999.2809.

59. Eaton, S.L., Murdoch, F., Rzechorzek, N.M., Thompson, G., Hartley, C., Blacklock, B.T., Proudfoot, C., Lillico, S.G., Tennant, P., Ritchie, A., et al. (2022). Modelling Neurological Diseases in Large Animals: Criteria for Model Selection and Clinical Assessment. Cells *11*, 2641. https://doi.org/10.3390/cells11172641.

60. Ella, A., Delgadillo, J.A., Chemineau, P., and Keller, M. (2017). Computation of a high-resolution MRI 3D stereotaxic atlas of the sheep brain. J. Comp. Neurol. *525*, 676–692. https://doi.org/10.1002/cne.24079.

61. J.I. Johnson, K.D.S., K.K. Davis, G.M. Kerndt, and B.M. Winn. The Sheep Brain Atlas. https://brains.anatomy.msu.edu/brains/sheep/index.html.